# Graphene-based Multimode Interference Device Design for Optical Switching Applications

Servaas T'jollyn

Supervisors: Prof. dr. ir. Dries Van Thourhout, Prof. Dr. Jose A. Lazaro (Polytechnic University of Catalonia)

Counsellor: Ir. Samael Sarmiento Hernández (Universitat Politècnica de Catalunya | UPC · Department of Signal Theory and Communications (TSC))

Master's dissertation submitted in order to obtain the academic degree of
European Master of Science in Photonics

Department of Information Technology
Chair: Prof. dr. ir. Bart Dhoedt
Faculty of Engineering and Architecture
Academic year 2017-2018

GHENT UNIVERSITY

# Master's Thesis

## Graphene-based Multimode Interference Device Design for Optical Switching Applications

author: Servaas T'Jollyn[†]

Guidance: Samael Sarmiento[⋆], Jose Lazaro[◇], Dries Van Thourhout[|]




Master in Photonics
UGent, UPC, VUB
27-08-2018

# Terms of use

# Acknowledgements

First and foremost I would like to thank my promotors Prof. Jose Lazaro, Prof. Dries Van Thourhout and my supervisor Samael Sarmiento for giving me the opportunity of working on the concept of coating an MMI with graphene and getting to know different modeling softwares and guiding me through my thesis.
I would also like to thank Dr. Koen Alexander, Dr. Zheng Wang and Prof. Roel Baets for answering my questions.
I would also like to thank my parents, my brothers and my friends for their support over the whole year.

Servaas T'Jollyn, September 2018

# Graphene-based Multimode Interference Device Design for Optical Switching Applications

Servaas T'Jollyn

Supervisor(s): Ir. Samael Sarmiento*, Prof. Dr. Jose Lazaro◇, Prof. Dr. Ir. Dries Van Thourhout†

*Abstract*—

**The relatively small size and low energy consuming switching potential offered by graphene-based electro-optic and electro-absorption switches has attracted a lot of attention in the photonics community recently and there has been no research on integrating graphene on an MMI so far to my knowledge. In this work, I theoretically model an integrated electro-optic switch based on a Multimode Interferometer (MMI) coated with graphene for data communication purposes. By varying a voltage over a range of 16V across a bi-layer of graphene, the proposed MMI can be used as a 1x2 switch with a graphene interaction length of around 140$\mu m$. As such, this component achieves a $0.22Vcm$ efficiency at $\lambda = 1550nm$, which is in line with efficiencies of similar components.**

**The MMI on itself, has low energy consumption and is intrinsically a low-loss component and thus the idea of using this proposed switch on a large scale in data communication as a splitter is not excluded.**

*Keywords*—**MMI Graphene Integrated Optics Fiber Optics**

## I. Introduction

WITH the increasing need for high-performance optical switches for use as optical interconnects, a lot of interest goes to graphene-based electro-absorbers and electro-modulators, because of the promising properties graphene has to offer. For instance, the refractive index of graphene can be easily changed over a wide range by altering its Fermi-level as shown in Figure 1([1]). Graphene's Fermi level can be manipulated by putting a voltage across it [5], [6]. Thus, by depositing a bi-layer of graphene on top of an MMI waveguide and putting a certain fixed voltage across the sheets, the refractive index of the structure can be changed. This allows us to change the beating pattern in the MMI and use the MMI as a 1x2 switch by alternating between 2 voltages.

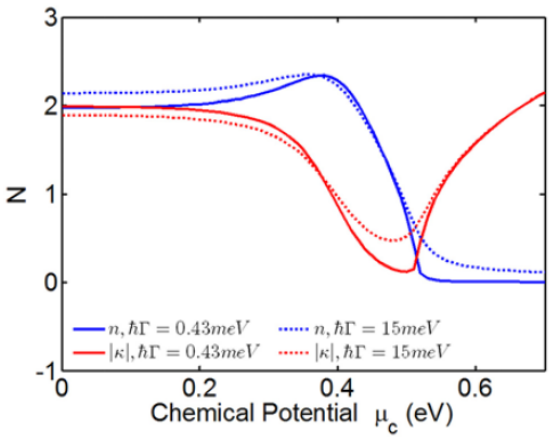


Fig. 1: Change of graphene refractive index with respect to the Fermi level

In this paper I show how an optimized design of the proposed MMI can lead to a switch that can compete with components that fulfill a similar function in the field of data communication. Furthermore, the efficiency of this component was tested and compared for different designs, ranging from different used materials to changes in waveguide design and graphene deposition. The standard design for the proposed MMI is shown in Figure 2.

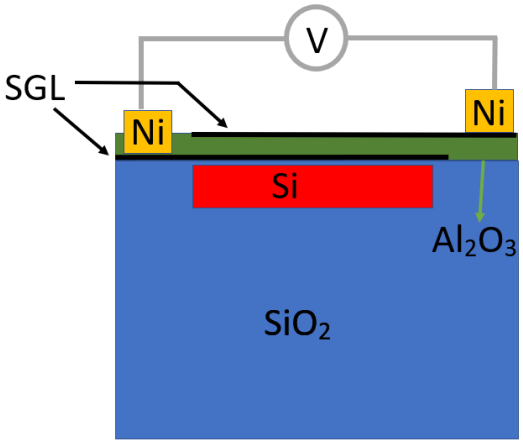


Fig. 2: Cross-section of a standard MMI design coated with a bi-layer of graphene

## II. Materials and Designs

### A. Materials

In *COMSOL* I tested various materials as waveguide and compared the functionality on the MMI. The materials I have tested as waveguide are: $Si$, $LiNbO_3$ and $SiN$. In Figure 3, I put the achieved change in refractive index and the losses for the best case, being a $Si$ waveguide on a $SiO_2$ cladding.

In order to explain why $Si$ yields the best results, I introduce here the beat length of an MMI which can be defined[2] as:

$$L_\pi = \frac{4n_r W^2}{4\lambda} \tag{1}$$

In this equation, $n_r$ and W are respectively the effective index and the width of the waveguide.

The results for $Si$ showed most promise, as the refractive index of $Si$, n=3.48 at $\lambda = 1550nm$, has the biggest refractive index contrast with the cladding, which is beneficial for how the MMI operates. This can be understood by noticing that a higher refractive difference between core and cladding leads to more compact designs and thus thinner waveguides due to the

increased optical confinement. With a less thick waveguide, the beat length($L_\pi$) of the MMI is shortened (see equation (1)) and thus, the required length for interaction with graphene is smaller.

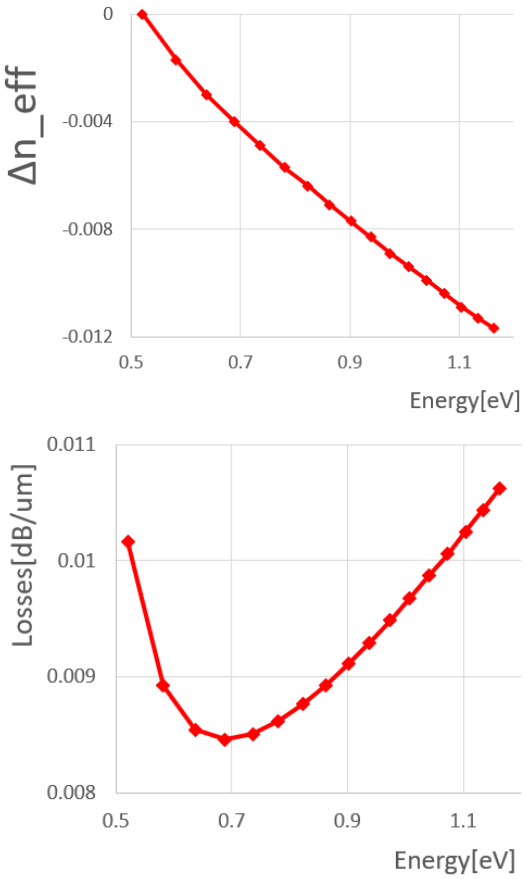


Fig. 3: Performance of the MMI design in Figure 2 with the $Si$ waveguide dimensions: 4000 nm x 220 nm, expressed in $\Delta n_{eff}$ vs Fermi level of graphene.

Because the interaction with graphene is relatively lossy ($\approx 0.01 \frac{dB}{\mu m}$), a shorter interaction length strongly reduces the overall losses. I note here that the results in Figure 3 are for a fundamental TM mode as input, because TM modes show the best mode overlap with graphene in this design made in *COMSOL*, as shown in Figures 10, 11.

### B. Designs

Firstly, a design was made where the DGL(double layer of graphene) and the 2 adjacent dielectrics are not deposited on top of the waveguide as in Figure 2, but rather about the middle of the waveguide (ratio 55% on top, 45% below), as shown in Figure 4.

This increased the coupling with the TE modes, but reduced the coupling with the TM modes. For the optimized ratio (55% on top, 45% below), the maximum coupling achieved with the TE modes closely approximates the coupling we get with the TM mode, shown in Figure5.

Secondly, a couple of graphene designs were made in *Lumerical* where not the entire surface is coated, but rather one or two

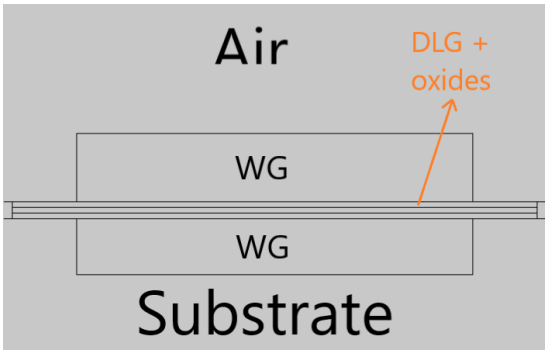


Fig. 4: Performance of TE in new design vs TM in original design expressed in losses vs Fermi level of graphene.

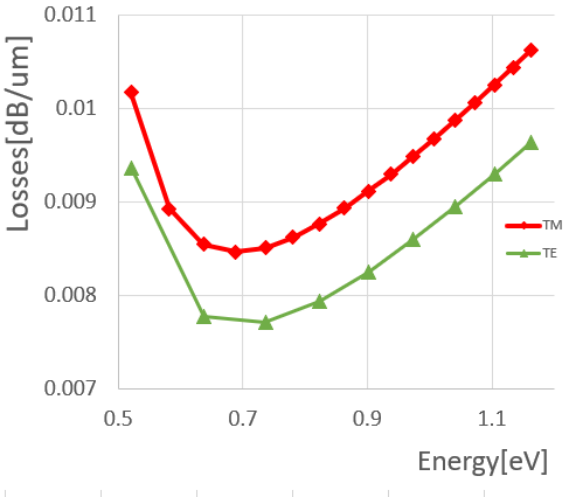


Fig. 5: Performance of TE in new design vs TM in original design, expressed in losses vs Fermi level of graphene.

sheets, as shown in the top view of the MMI in Figure 6. By searching an optimal value for the dimensions of these sheets, an increase in performance and thus a reduction of the required MMI length by a factor 14 was achieved. Briefly explained, the reason for this very big increase in performance is because the sheets were put over where the first order mode has its highest field intensities. Because of this, we can delay the first order mode with respect to the fundamental mode, and as such we make the difference in beat length a lot bigger between the two switching regimes. This basically yields a huge MMI length reduction.

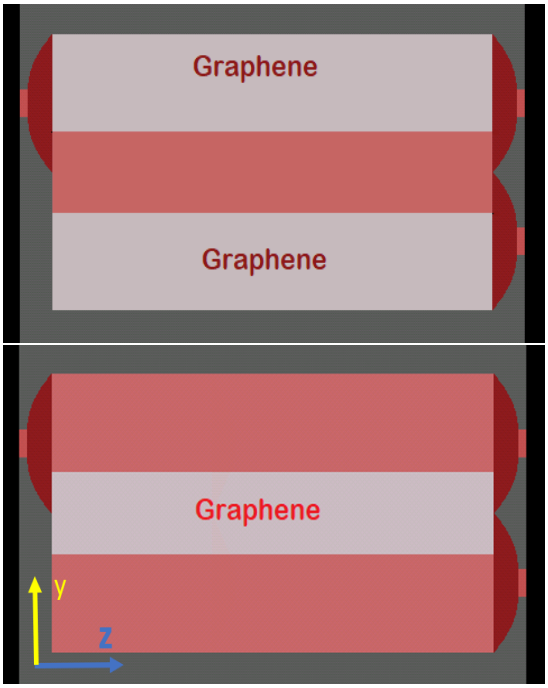


Fig. 6: graphene designs

## III. Results and Discussion

A design was made and optimized for TE modes, with the graphene and dielectrics deposited about the middle(0.45%-0.55%) of a 220 nm x 2000 nm $Si$ waveguide, based on the top design from Figure 6, where the bi-layer of graphene was deposited with a gap in the middle between the two sheets of $\approx 310\,nm$. The results of this design are shown in Figure 7.

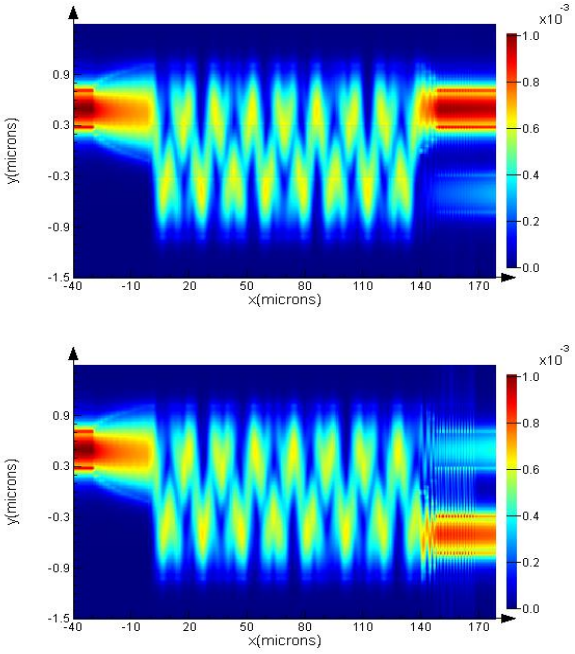


Fig. 7: Best achieved switching result

These results can still be somewhat optimized, by using the slightly better coupling TM modes, which I didn't add in the results due to practical difficulties with *Lumerical*. With calculations based on MMI length difference however, I predict of an efficiency increase of 4%.

From the results in *Lumerical*, there is a maximum loss of 0.4 dB due to the interaction with graphene. In reality there will be a lot higher losses, because losses due to sidewall roughness, propagation losses and losses due to defects in the used materials are not included in my model.

Lastly, in Figures 8 and 9, one can see the fractions of the input light that go to the different output ports, as well as the stability of the output when the used wavelength is changed for the two different switching regimes. These results were obtained in *Lumerical*.

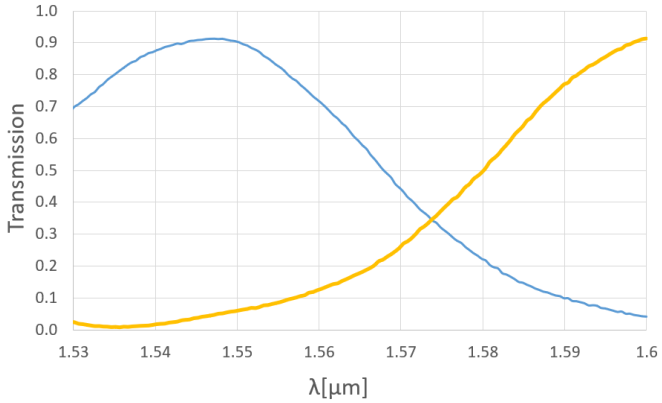


Fig. 8: Transmission of the input TE light to the upper output waveguide(blue) and the lower output waveguide(yellow) for a graphene Fermi level of 1.1636 [eV] (high voltage) versus wavelength

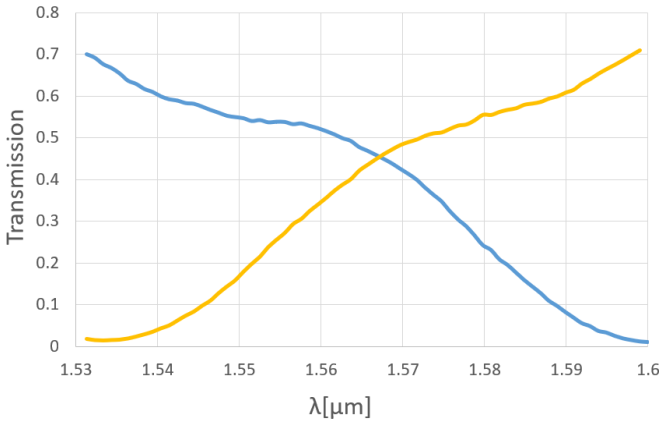


Fig. 9: Transmission of the input TE light to the lower output waveguide(blue) and the upper output waveguide(yellow) for a graphene Fermi level of 0.52 [eV] (low voltage) versus wavelength

The splitting here is not a perfect 50-50% and there is also some light leaking in the unwanted output. This can be actively remedied by putting graphene on the output waveguides and as

such introduce controlled losses. This is however an extra energy cost that can definitely be avoided by optimizing some parameters, such as the output port position or geometry and different tapering speeds for instance.

## IV. Conclusion

In the last design, a 139 $\mu m$ MMI coated with graphene was modeled that requires 16V difference to switch between the two output states. Consequently, this device has a $139\mu m \cdot 16\,V = 0.22V \cdot cm$ efficiency. This is quite in line with a similar graphene-based switch in literature [3], [4], where they achieve a somewhat lower efficiency of $0.28V \cdot cm$.

With a few more optimizations to the design, I believe it is a definite good candidate to experimentally test.

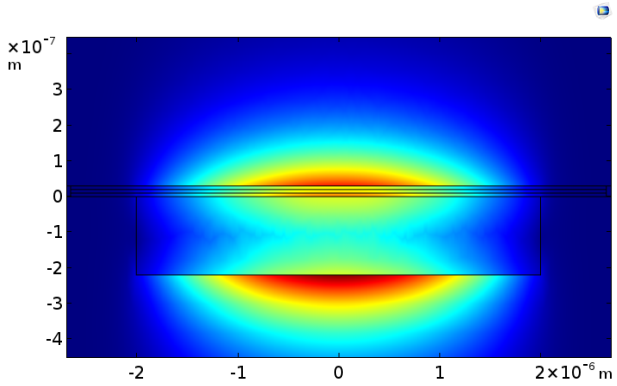


Fig. 10: Fundamental TM mode profile

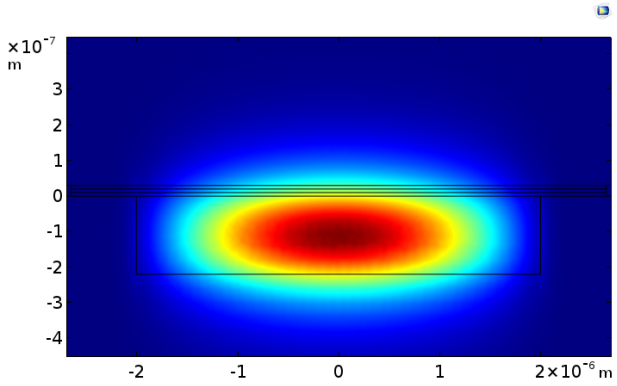


Fig. 11: Fundamental TE mode profile

## References


[1] Hu, Yingtao et al., "Broadband 10 Gb/s operation of graphene electro-absorption modulator on silicon: Broadband 10 Gb/s operation of graphene electro-absorption modulator on silicon, doi=10.1002/lpor.201500250", in Laser & Photonics Reviews **10**(2), pp. 307-316, 2016.

[2] "MMI Theory and Design", in University of Waseda, Honbun

[3] Romagnoli, M., "Highly Efficient Silicon Photonics Phase Modulator using Graphene", in Communications Conference and Exposition, Pisa

[4] Sorianello, V. and Angelis, G. De and Cassese, T. and Midrio, M. and Romagnoli, M. and Mohsin, M. and Otto, M. and Neumaier, D. and Asselberghs, I. and Campenhout, J. Van and Huyghebaert, C. Complex effective index in graphene-silicon waveguides doi = 10.1364/OE.24.029984

[5] Hanson, George W. Dyadic Green?s functions and guided surface waves for a surface conductivity model of graphene journal = Journal of Applied Physics,

[6] Li, Xuesong and Cai, Large-Area Synthesis of High-Quality and Uniform Graphene Films on Copper Foils, doi = 10.1126/science.1171245,

# Contents

# List of Figures

# List of Tables

# Acronyms

**AC** Alternating current.

**CMOS** complementary metal oxide semiconductor.

**DC** Direct current.

**DLG** Double Layer Graphene.

**EAM** Electro-absorption modulator.

**EOM** Electro-optic modulator.

**IR** Infrared spectrum.

**MEM** Micro Electro-Mechanical systems.

**MMI** Multimode Interferometer.

**SLG** Single Layer Graphene.

**SOI** Silicon on insulator.

**TE** Transverse Electromagnetic.

**TM** Transverse Magnetic.

**VIS** Visible spectrum.

# Chapter 1

# Introduction

## 1.1 General Introduction

OVER the last few decades, there has been an exponential development in computer and communication technology. In our arduous endeavour to make all technology faster and more accurate, the chip size has decreased and clock speed has increased tremendously. As such, data communication via copper interconnections was bypassed by the optical fiber used mainly nowadays as it has a larger optical bandwidth, less adjacent signal crosstalk, low fabrication cost, lower losses and, of course, CMOS compatibility [1, 2]. As the bandwidth of optical fibers is very large, the overall bandwidth of an optical fiber network is limited mostly by optical modulators and switches. They are thus the bottlenecks or key components of an optical network. Hence, investigation and improvement of these essential components is mandatory for the ceaseless evolution in the domain of data communication.
There are all sorts of different implementations of optical switches using for example MEMS, liquid crystals, acousto-optical methods, thermal methods, optical non-linearities, piezo-electrics... Because every switch has its pros and cons, it is valuable to search for alternative switches that perform well in different criteria.
In this thesis I explore if a Multimode Interferometer (MMI) coated with graphene can be used as an optical switch in data communication networks and I compare it to similar components that perform the same functionality.
An MMI coated with graphene can be used as a switch by putting merely two different fairly low DC voltages in the $[0V, 20V]$-range across the sheet of graphene to provide two different modes of operation in order to switch between output ports [3]. As changing this rather low voltage has low power

consumption and can be done very fast and precisely, the exploration of components coated with graphene could lead to a holy grail in data communication. To manipulate and guide light in optical fiber networks, we usually use state-of-the-art waveguiding dielectric materials that have a high index contrast (core-cladding). With this high contrast, we create a total internal reflection of the light within the fiber, guiding the light, with the least losses possible. In this work I focus on silicon photonics, as it is a field in which improvements are valued a lot, because it is the main link between electrical and optical processing due to CMOS compatibility. I do however also explore the performance of different materials such as LiNbO3, Al2O3, InP and GaAs. In the next section I will introduce the reader to the context of Silicon Photonics.

## 1.2 Introduction to Silicon photonics

Silicon photonics is the study and application of photonic systems which use highly purified silicon (up to 99.999% purity) as an optical medium [4]. The silicon typically lies on top of a layer of silica in what (by analogy with a similar construction in microelectronics) is known as silicon on insulator (SOI). Some other layouts are also possible, the most typical of which are shown in Figure 1.1.

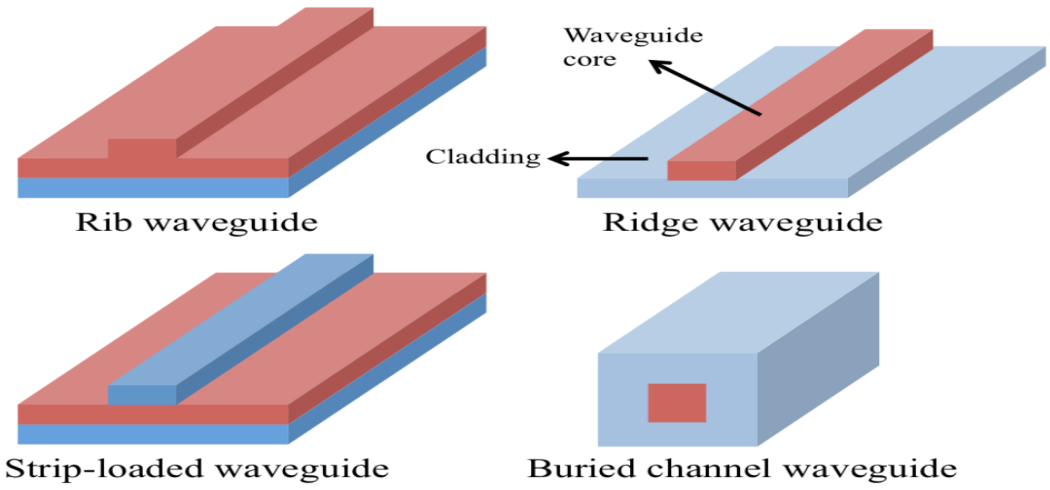


Figure 1.1: different types of waveguides[5]

Although silicon is not the best material for light generation, because of e.g. the indirect band gap, it is still used in many optical components as it can be fabricated very cheaply and is easily integrable with the prevalent CMOS technology because silicon is already used as the substrate for most integrated cir-

cuits, so it is possible to create hybrid devices in which the optical and electronic components are integrated onto a single microchip[6].

The first step in silicon photonics was to convert an electrical signal to an optical one, then guide the light in optical fibers, then convert the optical signal back to an electrical signal and process it. This conversion does not go without power and time losses. As such, silicon photonics has evolved and is still evolving to making all-optical networks, or integrating the electrical and optical components on the same small chip, rather than having them spread across multiple chips.

Nowadays it is becoming increasingly common that the patterns imprinted on silicon to make actual photonic components, have alignment tolerances of less than fifty nanometers [7]. This is largely sufficient for making an MMI, because it is rather insensitive to small geometrical errors.

Silicon photonics is a valid candidate for use in data communication, which works at a fixed central wavelength of $\lambda = 1550nm$ and Silicon has low propagation losses at this wavelength. However, an MMI can be fabricated with many different materials, including, but not restricted to: LiNbO3, Al2O3 on Si, InGaAsP/ InP and GaAs/ AlGaAs. As these materials all have different properties, investigation of an MMI coated with graphene is still a broad field and much research can be done to optimize this concept.

## 1.3 Introduction to Graphene

Graphene is a material discovered in 1962 by Hanns-Peter Boehm and his colleagues [8] that consists of a single layer of carbon atoms in a 2D plane, arranged in a honeycomb structure and is known to exhibit a variety of exceptional electronic and photonic properties (Figure 1.2); most prominant are its unique linear and gapless band dispersion which are highly desirable for photonic applications.

It was only until much later in 2010 that Geim and Novoselov got the Nobel prize for extracting the graphene from a piece of graphite such as is found in ordinary pencils. Using regular adhesive tape they managed to obtain a flake of carbon with a thickness of just one atom. This at a time when many believed it was impossible for such thin crystalline materials to be stable [9].

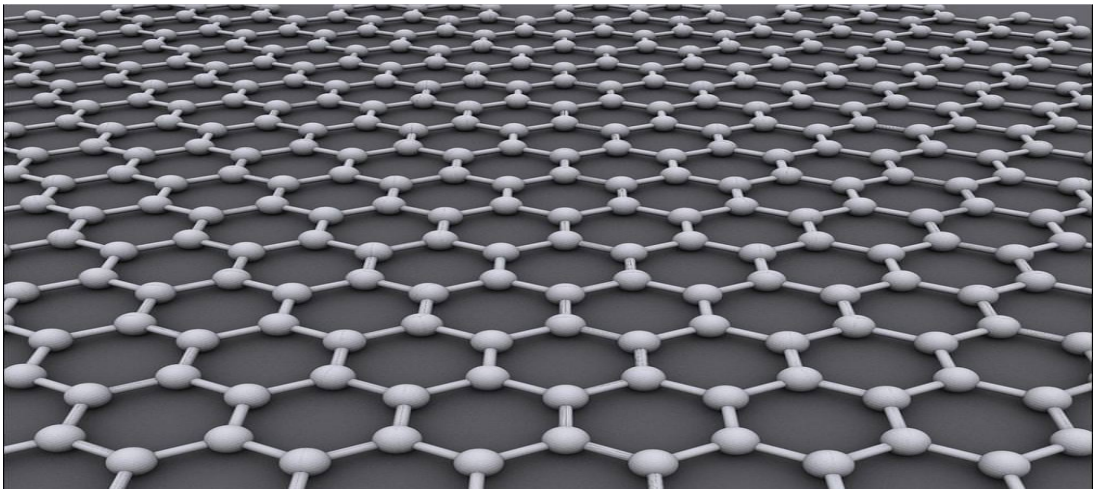

Figure 1.2: honeycomb structured graphene [10]

Graphene is defined as a semi-metal, because of its voltage-tunable properties that are a mix between common metals and common semi-conductors, as is shown in Figure 1.3.

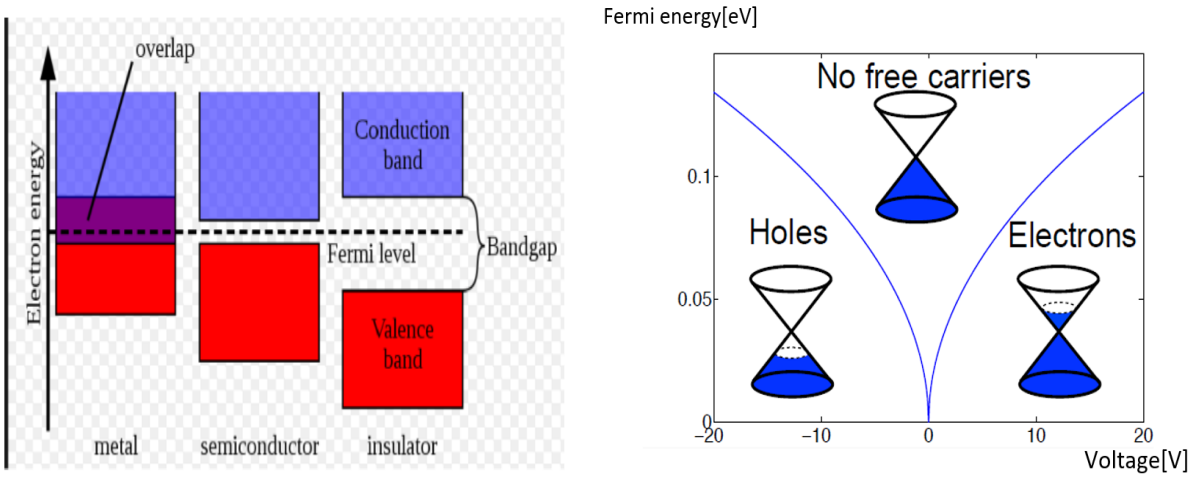


Figure 1.3: Classification of graphene as in-between metals and semi-conductors [11]

Some of the most extraordinary general properties include [1] ultra-wideband absorption, huge specific surface area, mechanical flexibility, exceptionally large thermal conductivity, voltage/doping controllable inter-band transition, saturable nonlinear absorption and high-mobility ambipolar carrier transport and even superconductivity has been observed in twisted bilayer graphene[12].

Additionally we have today the ability to produce high-quality graphene at wafer scale [13] and can transfer and integrate it onto heterogeneous substrates

and pattern it into planar devices. However, a major issue is that these properties are unobtainable or non-optimal in most investigated CMOS-compatible material systems thus far.

Despite this latter issue, incorporating graphene with Si-compatible photonics is a very promising approach toward the realization of practical high-speed, low-power photonic systems integrated with CMOS circuits.

In graphene, the energy-momentum relationship for electrons and holes is linear over a wide range of energies, rather than quadratic, so that both electrons and holes in graphene behave as massless relativistic particles with a very high energy-independent velocity. Graphene's band structure, together with its extreme thinness, leads to a pronounced electric field effect, which is the variation of a material's carrier concentration with electrostatic gating. Although the electric field effect also occurs in atomically thin metal films, these tend to be thermodynamically unstable and do not form continuous layers with good transport properties. In contrast, graphene is stable and has a nonzero conductance, even when charge carrier concentrations vanish. [14]

The fundamental optical properties of graphene can be most conveniently investigated with free-space optics using a normal incidence configuration as can be seen in Figure 1.4a).

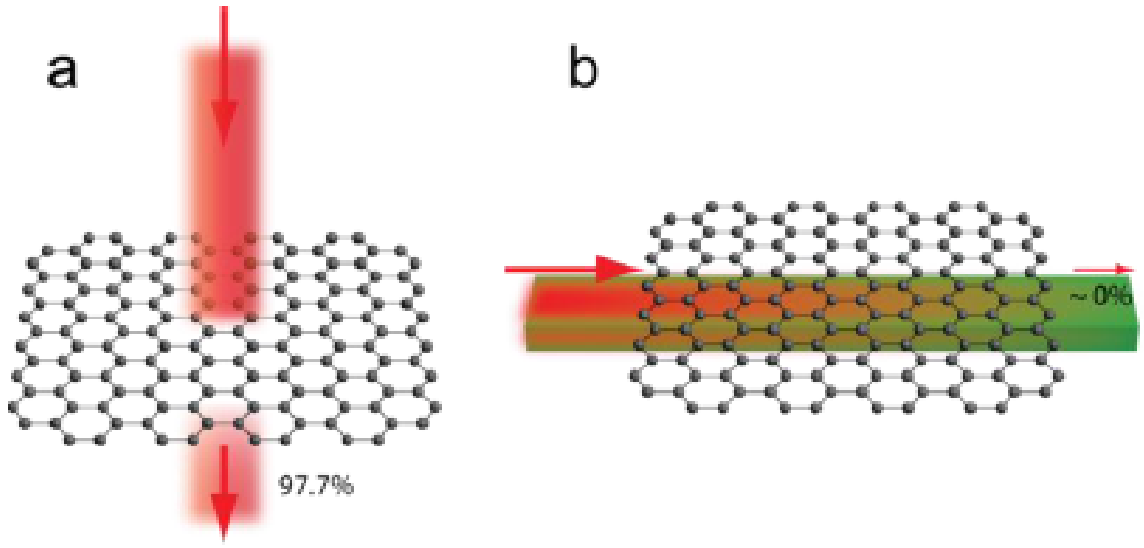


Figure 1.4: a) normal incidence, 2.3% absorption ; b) coplanar configuration, a possible 100% absorption when propagating long enough in graphene [15]

Graphene can be used either as an Electro-absorption modulator (EAM) and

as an Electro-optic modulator (EOM), depending on the amount of carrier doping in the material. In this thesis we would like to exploit both functions. This is worked out in chapter 3.

It is well known that when light is incident perpendicularly to a sheet of graphene for a very broad frequency range (VIS-IR), a sheet of one atom layer thick absorbs exactly 2.3% of the incident light and multiples of this per passed graphene layer ($\approx 1.1nm$). When propagating normal to graphene's surface, the light has a good spatial overlap with the graphene, but only a very small interaction length of one or a few atomic layers. However, by inserting the light coplanarly with the sheet of graphene as in Figure 1.4b), we can achieve a light-graphene interaction that is only limited by the length of the device, rather than the amount of graphene layers. This comes at the cost of a very small spatial overlap and thus less efficient coupling [15].

The formulas describing the light-graphene interaction for both setups can be found in Appendix B.

Nextly, shifting the Fermi level away from the center of the band structure, by either applying an external electric field, either through chemical doping, can suppress the optical losses in a layer of graphene due to Pauli blocking [16], as is depicted in the left part of Figure 1.5.
Due to Pauli blocking, the optical signal can pass through big lengths of graphene with a relatively low absorption with respect to the case with the central Fermi level. Due to the gapless nature of graphene, there are always carriers present at any Fermi-level. Thus changing the Fermi level, also readily changes the amount of carriers. This way, both the overall absorption and the amount of carriers can be tuned with the Fermi level.
On the right part of Figure 1.5, you can also see how the real and imaginary part of the refractive index change with respect to the Fermi level.

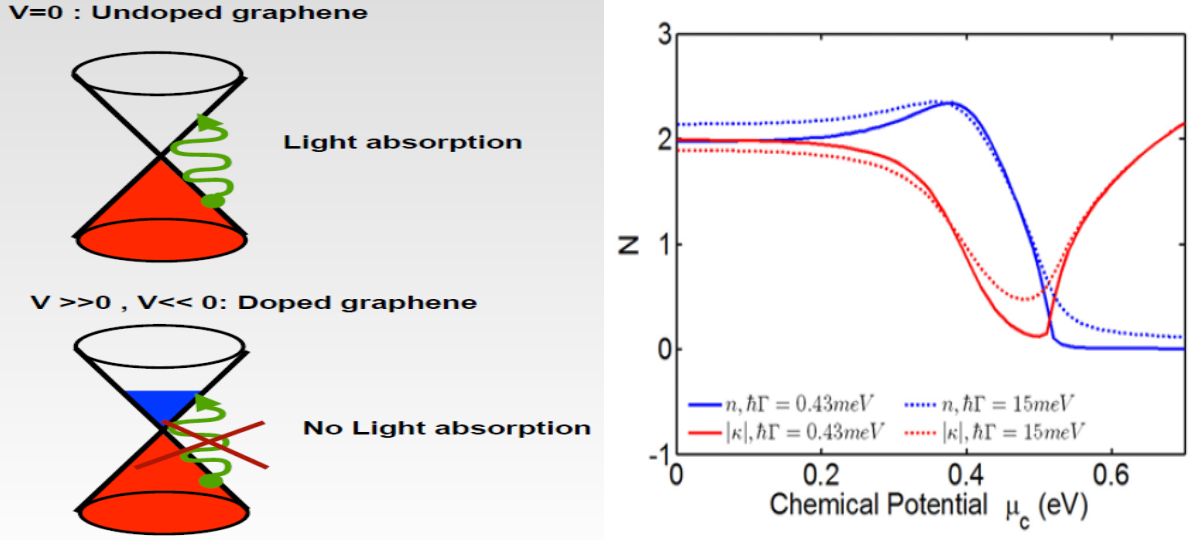


Figure 1.5: Left Figure: Band structure graphene: top=Fermi level at the center, bottom=shifted Fermi level [11]; Right Figure:change of refractive index of graphene with changing Fermi level [16]

Graphene is deposited on a surface commonly using the Chemical Vapour Deposition method (CVD) . CVD is a way of depositing gaseous reactants onto a substrate. The way CVD works is by combining gas molecules (often using carrier gases) in a reaction chamber which is typically set at ambient temperature. When the combined gases come into contact with the substrate within the reaction chamber (which is heated), a reaction occurs that create a material film on a substrate surface. The waste gases are then pumped out of the reaction chamber. For graphene, the substrate surface is usually Cu. Graphene then needs to be separated from the substrate to get stand-alone, which is a cumbersome problem. One way of realizing this is by dissolving the substrate in an acid. For Cu, it is possible to insert a thin layer of CuO between graphene and Cu that has weaker bonds with graphene and hence the graphene can be extracted more easily. This layer can then finally be deposited onto a substrate. This usually yields very high quality of the resulting deposited layer [17].

## 1.4 Introduction to MMI and couplers/switches

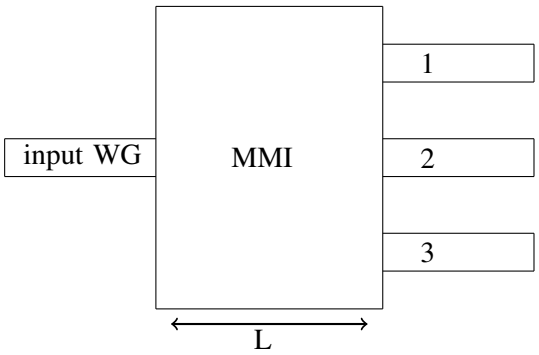


Figure 1.6: MMI scheme

A Multimode Interference device (MMI) is an optical component that falls under the category of optical couplers. A typical MMI has a waveguide structure that has larger dimensions than typical single mode waveguides, allowing multiple modes to coexist and interfere inside the waveguiding structure, like in Figure 1.7, where a single mode of light is incident from the left.

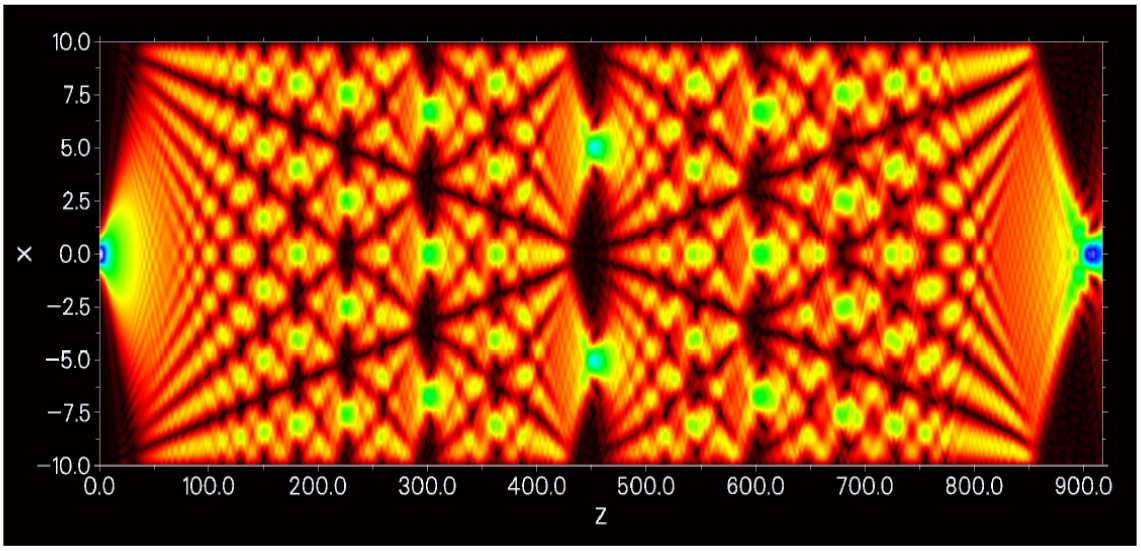


Figure 1.7: Visualization of the MMI working principle [18]

MMI's have their origin in the Talbot effect, a phenomenon first observed by H.F. Talbot in 1890. Talbot observed that if a monochromatic optical plane wave is incident upon a periodic diffraction grating, then the image of this grating will repeat itself at a fixed distance $L_T$ away from the diffraction grating.

Winthrop and Worthington extended the Talbot effect to two dimensional images. In doing so, they emphasized that the output image could be related to the input source via a convolution, and that the complex phase-amplitude of these images could be expressed as the sum of quadratic complex exponentials. Rivlin, and later Bryngdahl, suggested that by using total internal reflection in an optical fibre to replicate a periodic grating, it should be possible to induce a confined Talbot effect. This is the fundamental idea behind the MMI. MMI's are used extensively in photonic integrated circuits (PICs) due to their compact size, low loss, phase dependence and predictable performance.

There are more couplers, other than the MMI, such as its most famous brothers, the Y-junction ((Figure 1.8)) and directional couplers (Figure 1.9).

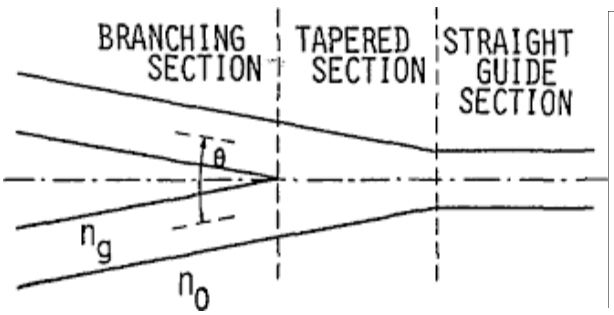


Figure 1.8: Y-junction scheme

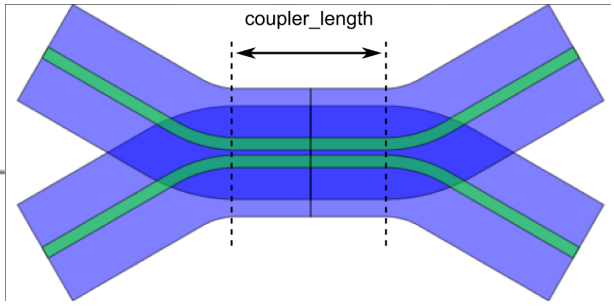


Figure 1.9: directional coupler scheme

The most common of couplers is the directional coupler that has the main issue of having low fabrication tolerances. A small variation in the gap between the two waveguides can drastically reduce the directional coupler's performance.
For a Y-junction, the biggest drawback is that it is very difficult to make a high index contrast Y-shaped branching section. These disadvantages are the main reason for the search of more suitable solutions such as the MMI.
The MMI couplers based on the principle of self imaging solves all these problems with properties such as compactness, high fabrication tolerance, inherent output power balance, polarization independence and low optical loss. This legion of advantages makes it clear that this coupler is the best option in the fabrication of more elaborated optical circuits.
These passive components are employed as power splitters and combiners in Mach Zehnder Interferometers (MZI) and optical switches, and in many other

applications, creating an increasing popularity in its use for integrated optical circuits.[19]

MMI's can be made in various different materials, such as LiNbO3, Al2O3/ SiO2 on Si, InGaAsP/ InP and GaAs/ AlGaAs among others. Not only the materials but also the design of MMI Couplers can have very exotic forms such as the designs in Figure 1.10. These 2 MMI designs are a 2x2 splitter with tapered walls and an Nx1 combiner with curved borders.

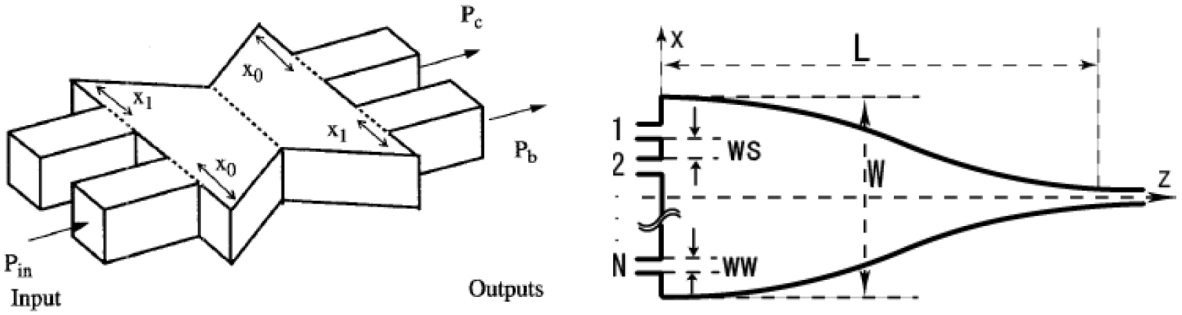


Figure 1.10: Exotic MMI schemes [20]

The MMI also fits in the family of switches, in which I will very briefly frame the MMI.
Firstly, thermal optical switches are based on the waveguide thermo-optic effect. Their main drawback is that they rely on varying temperatures, which intrinsically show exponentially decaying profiles, unless actively cooled. Switching speeds are thus capped at $\mu s$-ms-range.
A second group, the Electro-optical switches, such as the proposed graphene-coated MMI, realize optical switching functions by using electro-optic effects, which offer relatively faster switching speed compared to thermal optical couplers. Main types are $LiNbO_3$ switches, SOA-based switches, liquid crystal switches, electroholographic optical switches, and electronically switchable waveguide Bragg grating switches. They range in speed between ps and ms switching speed.
Thirdly, all-optical switches realize switching functions relying on intensity-dependent nonlinear optical effects in optical waveguides. Their main drawback is that they usually require high operating powers. Lastly, switches based on optical MEM's are distinguished in being based on mirrors, membranes and planar moving waveguides. Their main drawback is that they use movable parts

to switch the light. Mechanical movement is intrinsically slow and introduces damping noise. They have speeds varying between hundreds of ns to ms [21].

## 1.5 Objective of the thesis

The goal of this thesis is to explore theoretically whether an MMI can be used in combination with graphene to make a switch for mainly data communication applications. After verification that the concept is valid, new, realistic designs and ideas are brought to the table to enhance its performance so that it might compete with currently available switches.

## 1.6 Thesis outline

The idea behind this thesis is to test how graphene, a recently discovered material, can alter the behaviour of a component that is well-known, the MMI, in order to come up with a combined component that can offer an advantage to currently existing devices used in data communication that perform similar functions. So, in this work, the MMI is placed firstly in the larger context of splitters, combiners, switches and couplers. Secondly, the study explores how graphene works and how we can use its properties to our advantage and enhance the MMI's properties.

In order to describe properly how the interaction between graphene and the MMI works, a mathematically rigorous background is given of the MMI that can explain its behaviour and how the intertwining with graphene can modify this behaviour to make the MMI function as a switch.

The study then requires the testing of different designs of the proposed MMI to see which parameter can improve the switching behaviour. There are two major parts that can be optimized or changed, namely the coupling with graphene and the behaviour of the MMI.
To increase the coupling with graphene, we explored sending in light of different polarization and wavelength, changing the distance that the sheet of graphene is separated from the MMI, changing the thickness of both the MMI and graphene, together and separately and changing the temperature.
Then, to change the behaviour of the MMI, we changed the used materials for

the waveguide, for the cladding, the standard layout of the MMI and varied tapering lengths and profiles.

After the designing process, the results are compared from the different ideas and they are then briefly discussed.
Now it is important to relate the findings and results to currently used and tested components and place the proposed MMI in a broader view of similar components once again.
Finally, we reflect on the results to see if this is a component worthy of experimentally constructing and what could be improved in the future to make the proposed MMI more efficient.

# Chapter 2

# Multimode Interferometer Couplers

The basic idea of Multi-Mode Interference (MMI) is abruptly increasing a single mode waveguide's thickness, allowing multiple higher order modes to co-propagate and beat in the waveguide. This component can be used for multiplexing the signal into $n$ different paths ($n \in \mathbb{N}$) by using the fact that every mode travels at a different speed and higher order modes have their energy laterally spread over different nodes. As a result, we get z-dependent lateral standing wave profiles as a consequence of beating of various modes. By picking the length of an MMI wisely, you can guide a node of high Electrical field in the MMI out as single guided modes in the output waveguides.

MMI's have a higher tolerance to dimension deviations in fabrication process than most other optical couplers [22] and (thus) are produced also more easily as compared to directional couplers which require sub-$\mu m$ gaps. Additional perks to using this component is that it's inherently a low-loss component and has a large optical bandwidth [23]. A downside to standard MMI's is that back reflections can be very efficient, because they follow the same self imaging principle as in the forward direction in the MMI [20]. This can however be remedied by smartly tweaking the design, by for instance making the input and output sidewalls slanting instead of perfectly straight.
Furthermore the losses of the component can be reduced by making the transitions into and out of the MMI smoother by means of tapering (see Figure 3.1). Tapering effectively enhances mode overlap between single mode and MMI, yielding less losses [24]. Tapering is further worked out in section 3.1.

In order to test and comprehend the internal behaviour of light in an MMI coated with graphene, the behavior of a normal MMI is mathematically studied in following sections and compared with *COMSOL Multiphysics software* and

*Lumerical Mode Solutions* in order to get reproducible results that comply with prior art.

## 2.1 Practical results on regular MMI

For clarity, I define the propagation axis to be the z-axis, the width of the MMI, the y-axis and the height, the x-axis as shown in Figure 2.1.

As rigorously explained and proven later in this section, the resulting beating pattern in the MMI can be described with just a few parameters of interest to our cause.

$$W_e \approx W_M + \frac{\lambda_0}{\pi}\left(\frac{n_c}{n_r}\right)^{2\sigma}\left(n_r^2 - n_c^2\right)^{\frac{-1}{2}} \tag{2.1}$$

$$L_\pi = \frac{\pi}{\beta_0 - \beta_1} \approx \frac{4 \cdot n_r \cdot W_e^2}{3 \cdot \lambda_0} \tag{2.2}$$

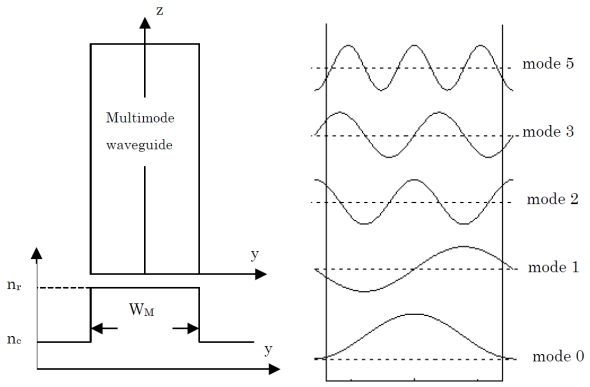


Figure 2.1: MMI, $n_{eff}$ and supported modes [25]

$W_M$ is the actual width of the MMI structure as shown in Figure 2.1. $W_e$ on the other hand is the average effective width that the propagating modes feel. In general the widths $W_e$ can be approximated by the effective width $W_{e0}$ corresponding to the fundamental mode. $\lambda_0$ is the vacuum wavelength, $\sigma = \begin{cases} 1, & \text{TM.} \\ 0, & \text{TE.} \end{cases}$. $n_c$ is the refractive index of the cladding and and $n_r$ is the refractive index of the core. $L_\pi$ is defined as the beat length of the 2 lowest order excited modes.

For a non-symmetrical MMI (input port is not centered at y=0, see Figure 2.2), the propagating modes cause a beating pattern that periodically mirrors the input field at a certain distance around y=0 and also periodically reproduces the input field after a certain other distance [20]. This property is just what we handily use to switch the signal between 2 output ports. The behaviour is schematically shown in Figure 2.2 and in (modeled) reality in Figure 2.3.

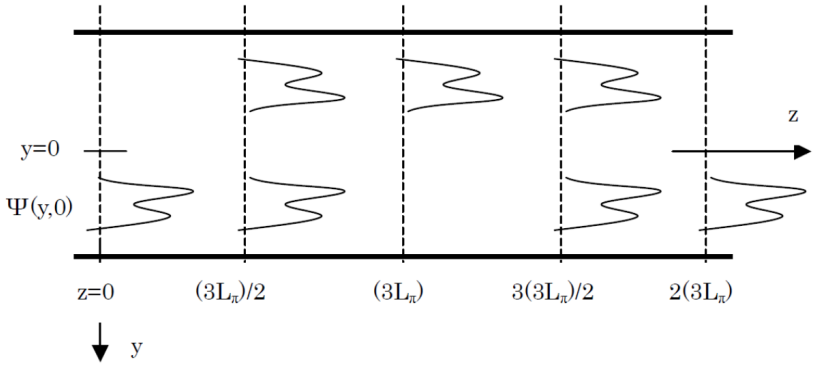


Figure 2.2: Scheme of the behaviour of a non-symmetrical MMI [20]

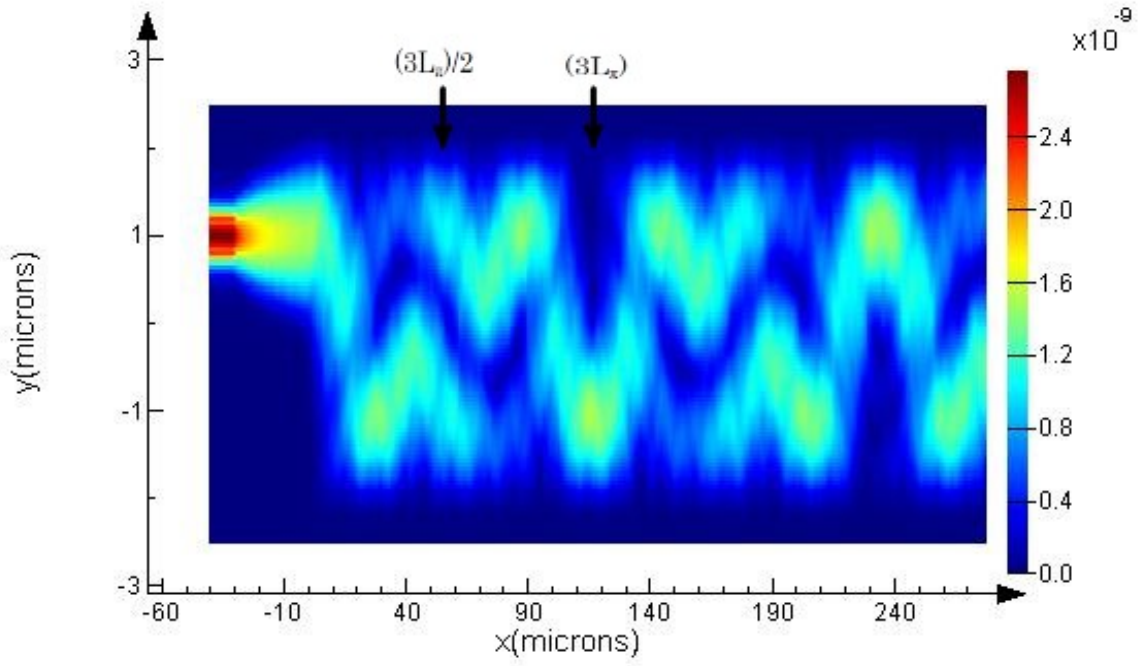


Figure 2.3: Field intensity mirroring in MMI

I tested this behaviour with *COMSOL* for a symmetrical MMI purely to visualize the MMI beating behaviour (Figure 2.4). Note that the symmetrical

MMI is a degenerate case of the non-symmetrical one, as mirroring the input field around y=0, yields the field itself (if your original input was symmetrical of course). The beating pattern for the symmetrical MMI can be seen in Figure 2.4.

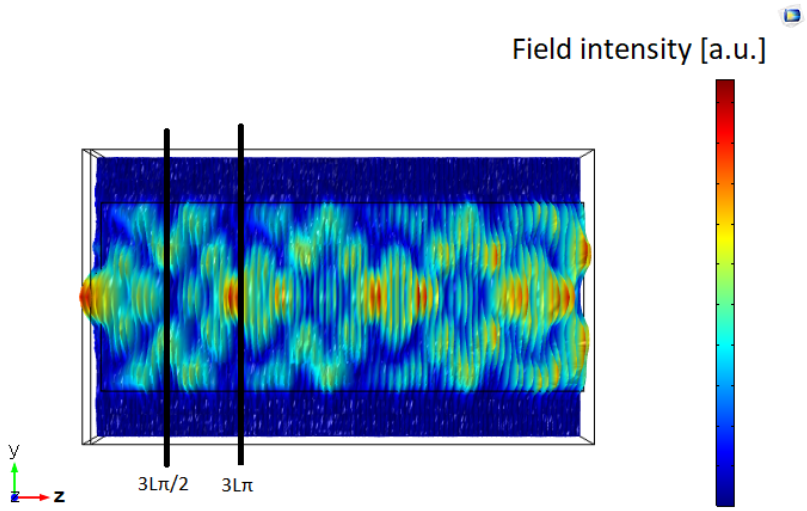


Figure 2.4: Visualization of the MMI beating pattern

In *Lumerical*, the behaviour of a non-symmetrical MMI was tested for a 0.22 $\mu m$ x 4 $\mu m$-thick MMI with a *Si* waveguide on $SiO_2$ cladding. We can calculate the beat length $L_\pi$ from equation (2.2), given the 2 lowest order propagation constants, as calculated by *Lumerical*:

$$\beta_0 = 11.4437[\mu m^{-1}] \tag{2.3}$$

$$\beta_1 = 11.3670[\mu m^{-1}] \tag{2.4}$$

This yields an $L_\pi$ of 40.98 $\mu m$. We should thus see that the image is split in 2 at 1.5*$L_\pi \approx 60\mu m$ and mirrored at 3*$L_\pi \approx 120\mu m$ in Figure 2.3. This resulting mode profile thus agrees very well with theory.

## 2.2 Theoretical derivation of MMI as switch

The behaviour of the basic MMI can be properly described in 2D because in the $3^{rd}$ dimension, the light in the waveguide remains single mode (this is the x-axis).

The way light behaves in the MMI structure is governed of course by Maxwell's equations:[1]

$$\vec{\nabla} \times \vec{E} = -\frac{\partial \vec{B}}{\partial t} \tag{2.5}$$

$$\vec{\nabla} \times \vec{B} = J + \frac{\partial \vec{D}}{\partial t} \tag{2.6}$$

$$\vec{\nabla} \cdot \vec{B} = 0 \tag{2.7}$$

$$\vec{\nabla} \cdot \vec{D} = \rho \tag{2.8}$$

$$\tag{2.9}$$

Since we only work with quasi monochromatic TE/TM waves ($\lambda \approx 1550nm$), we can reduce Maxwell's equations to the Helmholtz equations:

$$\frac{\partial^2 E_{x,m}(y)}{\partial y^2} + \left( k^2 \cdot n(y)^2 - \beta_m^2 \right) = 0 \tag{2.10}$$

Here k is the free space wave number, $E_{x,m}(y)$ is the mode profile for mode m, $\beta_m$ is the propagation constant for mode m. This equation can be solved by finding the proper Eigenvalues of the system. The field profile should thus be represented in the system's Eigenmode basis as a sum of the Eigenvectors of the MMI structure.When we assume that the spectrum of the input signal is narrow enough not to excite any radiating modes(or such a small amount that they can be neglected), this leads to:

$$E_{x,m}(y) = \sum_{m=0}^{\infty} a_m \, \psi_m(y) \tag{2.11}$$

Here, $a_m$ is defined as:

$$a_m = \int E_x(y) \psi_m(y) dy / \int \psi_m(y) \psi_m(y) dy \tag{2.12}$$

[1] The following derivations are loosely based on the derivations in a paper on the theory of standard MMI's [18]

The field profile at a distance z can then be written as a sum of all the guided modes:

$$E_x(y,z) = \sum_{m=0}^{\infty} a_m \psi_m(y) e^{j(\omega t - \beta_m z)} \tag{2.13}$$

When we take the phase of the fundamental mode (exp(-j $\beta_0$)) as a common factor out of the sum, this will not change the result, as it is just a phase factor in the orthogonal basis, so we may drop this.
Furthermore, for the quasi monochromatic waves, $\omega$ is a constant and thus we can assume the only-time-dependent factor exp(j$\omega$ t) implicit hereafter. With these modifications, the Electric field profile at a distance $L$ can be handily rewritten as:

$$E_x(y,L) = \sum_{m=0}^{\infty} a_m \psi_m(y) e^{j(\beta_0 - \beta_m)L} \tag{2.14}$$

Now, I introduce the constant $L_\pi$, which I will use to substitute a part of equation (2.14).

The lateral wavenumber $k_{y,m}$ and the propagation constant $\beta_m$ are related to the effective index $n_r$ by the dispersion equation:

$$k_{y,m}^2 + \beta_m^2 = k_0^2 n_r^2 \tag{2.15}$$

The standing wave condition in y-direction is:

$$k_{y,m} W_{e,m} = (m+1)\pi \tag{2.16}$$

Here, $W_{e,m}$ is the effective waveguide width for mode m, which, under the condition that there are many propagating modes in the MMI [18], can be approximated by the actual width of the MMI: $W_e \approx W_{e,m}$. By substituting equation (2.16) in (2.15) and solving for $\beta_m$, we get:

$$\beta_m = \sqrt{n_r^2 \cdot k_0^2 - \left(\frac{(m+1)\pi}{W_{e,m}}\right)^2} \approx n_r \cdot k_0 - \frac{(m+1)^2 \pi \lambda}{4 n_r W_{e,m}} \tag{2.17}$$

By taking the first order Taylor expansion of $\beta_m$ and substituting this in the

definition, I finally arrive at $L_\pi$ :

$$L_\pi = \frac{\pi}{\beta_0 - \beta_1} \approx \frac{4 \cdot n_r \cdot W_e^2}{3 \cdot \lambda_0} \tag{2.18}$$

Now equation (2.14) can be more elegantly written as:

$$E_x(y,L) = \sum_{m=0}^{\infty} a_m \, \psi_m(y) e^{j(\frac{m(m+2)\pi}{3L_\pi})L} \tag{2.19}$$

By inspecting this Electrical field profile, we see that E(y,L) will be an image of E(y,0) whenever:

$$e^{j(\frac{m(m+2)\pi}{3L_\pi})L} = 1 \tag{2.20}$$

or

$$e^{j(\frac{m(m+2)\pi}{3L_\pi})L} = (-1)^m \tag{2.21}$$

The first equality means that the phase changes of all the guided modes at distance L differ by integer multiples of $2\pi$. In this case, all guided modes have undergone a phase change that is a multiple of $2\pi$ and thus interfere with the same relative phases they had in z = 0. The field at z=L is thus a perfect image of the input field.
The second equality means that all the even modes have undergone a phase change of multiples of $2\pi$, while the odd modes have undergone a phase change of multiples of $2\pi + \pi$. Because of this, the interference produces an image mirrored with respect to the plane y = 0.
Due to the periodic character of the Electric field inside the MMI, direct and mirrored single images of the input field $E(y,0)$ will therefore be formed by interference of all guided modes at distances z that are, respectively, even and odd multiples of the length $3L_\pi$.

## 2.3 Graphene-coated MMI: length calculations

We know from equation (2.19) that the Electrical field in the MMI at a distance z may be written as:

$$E_x(y,z) = \sum_{m=0}^{\infty} a_m \, \psi_m(y) e^{j(\frac{m(m+2)\pi}{3L_\pi})z} \tag{2.22}$$

Together with the non-symmetry of the MMI structure this leads to the following distances for z:

$$L_{odd} = 3(2k+1)L_{\pi} \tag{2.23}$$
$$L_{even} = 3(2k)L_{\pi} \tag{2.24}$$

for any $k \in \mathbb{N}$. Here, $L_{odd}$ is the condition for the distances at which the input mode is mirrored around $y = 0$ and $L_{even}$ is the condition for exact copies of the input field.
As the MMI is to be used as a switch, we want the MMI length to be such that with a low voltage across the graphene, there should be an exact copy of the input at the output, while for an high applied voltage, there should be a mirrored image at the output as is shown in Figure 2.5.

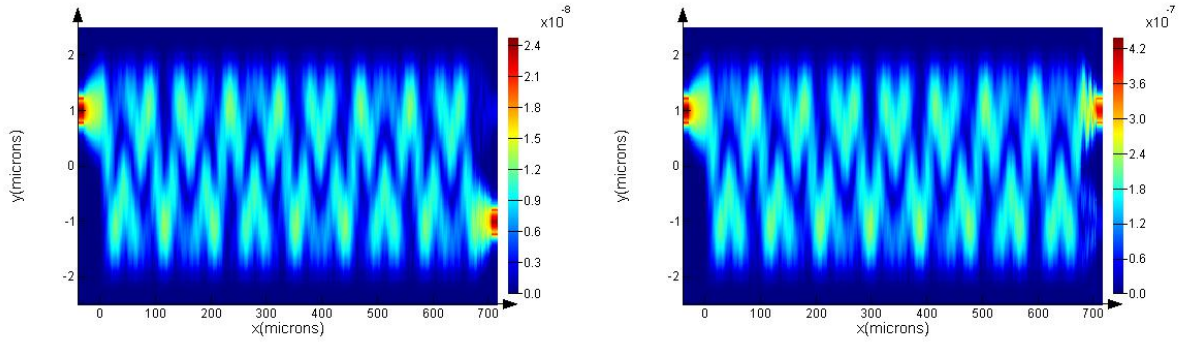


Figure 2.5: The 2 MMI switch regimes

As such, we rewrite (rename) the above equations to satisfy this condition:

$$\begin{aligned} L_{odd} &= 3(2k+1)L_{\pi,lowV} \\ L_{even} &= 3(2k)L_{\pi,highV} \end{aligned} \tag{2.25}$$

This leads to the requirement that $L_{odd}$ be equal to $L_{even}$ for a certain k $\in \mathbb{N}$. Lastly, we substitute the definition of the propagation constant ($\beta_m = n_{eff,m} \cdot k_0$) in equation (2.2) for the 2 beat lengths of interest:

$$L_{\pi,low} = \frac{\pi}{k_0(0, n_{lowV} - n_{1,lowV})} \tag{2.26}$$
$$L_{\pi,high} = \frac{\pi}{k_0(n_{0,highV} - n_{1,highV})} \tag{2.27}$$

Here, $n_{0,lowV}$ and $n_{1,lowV}$ are the refractive indices for the fundamental mode and the the first order mode with a low voltage across graphene.

The refractive indices for the different modes can be calculated in simulating software and then, with these values, we only need to solve this set of equations (2.25) for an integer k.

As an introduction to why we look for new designs in the following chapter, I calculate the MMI length here for the standard design(Figure 3.1) and show the resulting field profile. With the theoretical results that can be found in table 4.1 for a $Si$ on $SiO_2$ MMI, and $W_e = 4\mu m$, this yields an MMI length of:

$$L_{MMI} = 8.897[mm] \tag{2.28}$$

With this MMI length of $\approx 9$ mm, the field profile evolves as can be seen in Figure 2.6. As low as the losses may relatively be, after a propagation of several millimeters, the signal is obliterated. Because of these huge losses, it is clear why this basic model needs some refinements.

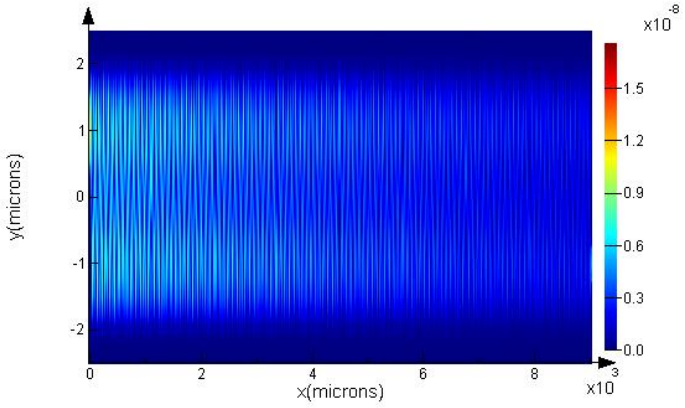


Figure 2.6: Losses completely destroy the signal after propagation over 9mm in the MMI coated with graphene

# Chapter 3

# Design of an MMI coated with graphene

Since electro-optic effects are so weak in Silicon, common modulators operate over a narrow bandwidth, are slow and can become quite large in dimensions, even up to mm's, which is unacceptable for chip integration. This is where graphene based modulators step in to overcome these limitations with its high carrier mobility and gate-controllable conductivity.

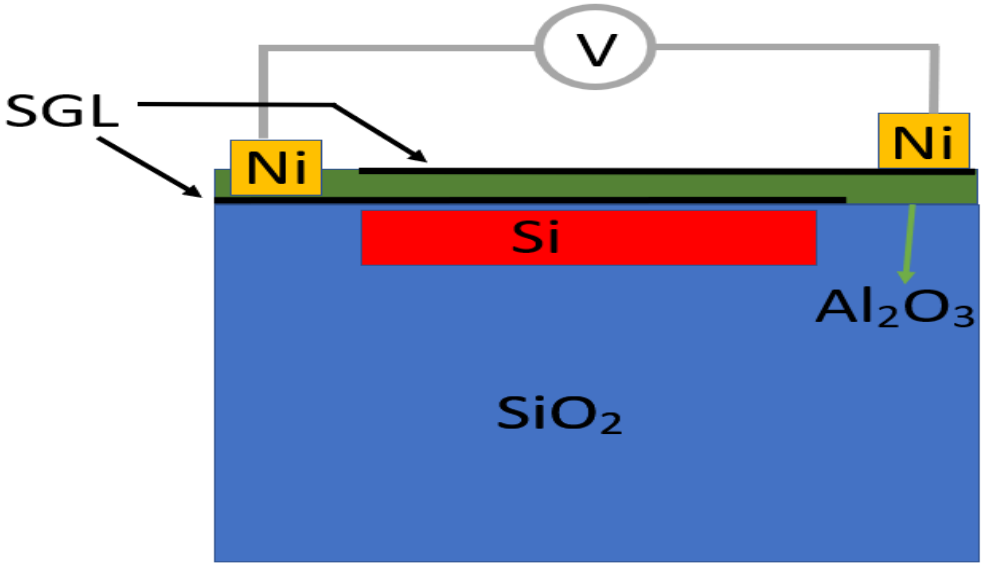


Figure 3.1: Design of GOS structure: cross section

A typical single layer graphene integration on silicon is configured as a graphene-oxide-silicon (GOS) structure, as shown in Figure 3.1. I designed this cross-sectional profile with a $SiO_2$ substrate and a $Si$ waveguide. As a small spacer between the waveguide and a lower layer of graphene, there is a small

dielectric layer of $SiO_2$. The two single layers of graphene (SLG) are spaced by a layer of $Al_2O_3$. The layers of graphene are put into contact with metal islands, Ni chosen here (because [26]), to be able to apply a voltage to graphene's surface.

Mostly because a similar design has already been experimentally tested, I use this as it gives a good reference of a component for which we know how it behaves in reality [27].

In Figure 3.2, different standard and stylized designs are presented for guiding the light.

In the case of an MMI coated with graphene, I first chose the rib or ridge structure for the design. This kind of waveguide approach provides some significant advantages compared to strip or buried waveguides as it allows for enhanced flexibility and compatibility with all processing modules such as photodiodes and multiplexers [28]. However, because it is easier to deposit graphene on a flat surface (the graphene can break when making the transition in height between waveguide and substrate), the second and final design choice was an in-between of the ridge and the buried channel. We bury the ridge just enough so that the top surface of the ridge coincides as well as possible with the top surface of the substrate(see Figure 3.1).

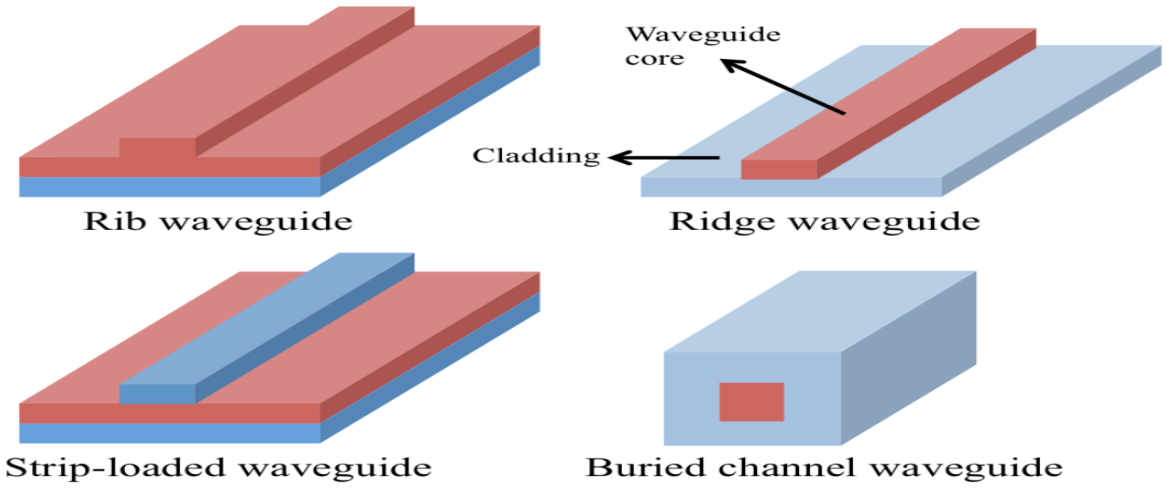


Figure 3.2: different types of waveguides[5]

The ridge deposited on top (and thus not buried as described above) would be preferable for the MMI, as the beat length between the modes is sped up because of the resulting lower average refractive index (see equation(2.2)). The confinement losses would also be slightly smaller upon propagation, because

there is more optical confinement in the core as the ridge sees 3 sides of air. However, there can also be a lot of scattering losses on high index contrast sidewalls. I cannot take this latter effect into account as it is not implemented in *Lumerical* or *COMSOL* and is mostly due to fabrication errors and should thus be tested experimentally.
However, if the ridge can be deposited on top with high accuracy then sidewall scattering losses may be very low and this design could lead to a slight improvement of the result: the change of refractive index that reduces the beat length in the MMI, and the reduced losses upon propagation are assumed very small, but it may be worth to test it, in order to improve efficiency.

In my designs, I thus keep the ridge-shallowly-buried-inside-substrate layout.

Having chosen the waveguide structure, we deposit graphene on top, embedded in dielectric layers, displayed in Figure 3.1. This design was optimized for TM modes because of two reasons. On one hand, guided TM modes (or quasi-TM modes) show hybrid modes that have an Electrical field component in the propagation direction and can thus couple to graphene. This is because light that has a perpendicular polarization to the plane of graphene has no coupling to it.
On the other hand it is proven to be feasible to fabricate a design with graphene on top of a waveguide where TE modes have an Electrical field zero-node, whereas TM modes show a maximum of the Electrical field at the top.

## 3.1 Tapering

The first optimization to the standard design is to taper in and out of the MMI by tapering the in- and output waveguides.
Tapering increases the overlap between the guided modes in the MMI and in the in- and output waveguides.
As the mode propagation constant is defined as:

$$\beta_i \approx k_0 n_r - \frac{(i+1)^2 \pi \lambda_0}{4 n_r W^2} \tag{3.1}$$

, the number of modes present in the waveguide grows or decreases quadratically with the waveguide width. Higher order modes that stop guiding in

narrower waveguides, give their energy to lower order modes or to radiating modes. The more gentle the transition between the change of waveguide width, the less energy is lost to radiating modes. The most efficient tapering would be a parabolic tapering, as its width grows tailor-made to the newly created propagating modes. Linear tapers on the other hand do this job equally well, however at the cost of having to taper over a longer distance (Figure **??**).

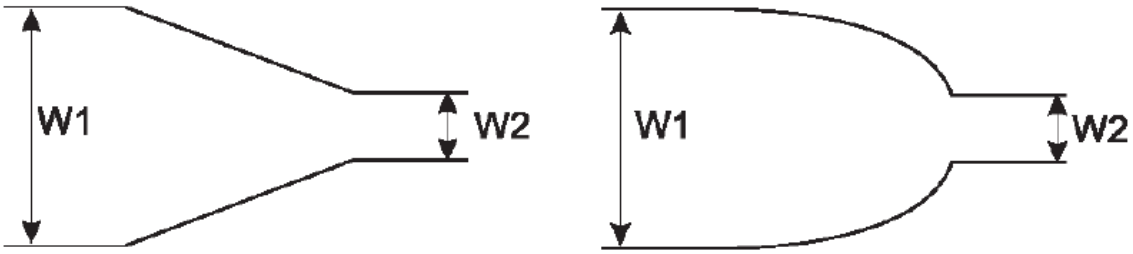


captionThe linear and parabolic tapering[25]

Tapering brings along two extra benefits for the MMI. Firstly, at sharp profiles or corners with abrupt discontinuities, reflections tend to build up. Tapering reduces these sharp corners or abrupt discontinuities, reducing these unwanted reflections. Secondly, tapering causes adjacent waveguide outputs to experience less overall crosstalk because the gap between the waveguides changes along propagation. As such, no standing constructive interference is maintained between two adjacent waveguides [19].
It is thus important to select a good tapering profile to increase the overall behaviour of the MMI and to protect components that are sensitive to back reflections.

Coupling losses can be completely annihilated by tapering-in in such a way that all the energy in the fundamental mode before tapering are gradually passed on to all the excited modes during the tapering, with no energy being lost to radiating modes (and vice versa for tapering-out). This kind of tapering is called adiabatic tapering and should always be striven for if the device length on small integrated chips allows it .

Concretely, the tapering occurs from a single mode waveguide width to maximum half of the MMI width. Tapering to a somewhat smaller width than half of the MMI width is not unwanted, because the structure where the 2 adjacent

waveguides would meet in the middle of the MMI, is just like the Y-junction, which is difficult to manufacture.
As such, I calculate the maximum coupling length for a $Si$ on $SiO_2$ MMI with a width $W_M = 4\mu m$ and a tapering to $2\mu m$ with an antisymmetric input as shown in Figure 2.3.
Important here is that the tapering length is different for TE and TM modes. The fundamental TM mode is tapered in a symmetrical way and will thus not excite the fist order asymmetrical TM mode. As such, the values are obtained for the fundamental TM and the second order symmetrical TM. With values obtained in *Lumerical*, this yields:

$$z_{coupling,TM} = \frac{\pi}{k_0 n_1 - k_0 n_2} = \frac{\lambda}{2(1.89340 - 1.61551)} = 2.79[\mu m] \tag{3.2}$$

For excited TE modes, a similar story can be told, and the resulting coupling length is shown below:

$$z_{coupling,TE} = \frac{\pi}{k_0 n_1 - k_0 n_2} = \frac{\lambda}{2(2.81034 - 2.58786)} = 3.48[\mu m] \tag{3.3}$$

So any tapering with a larger tapering length than $z_{coupling}$ will give a perfect coupling.

## 3.2 Crosstalk reduction

Due to the principle of Pauli blocking, the graphene layer can be made completely optically transparent by shifting the Fermi level away from either conduction or valence band (by either doping or applying a voltage). If the shift is big enough, the passing light does not carry enough energy to excite graphene's electrons or holes for interband absorption. This is visually presented in Figure 3.3.

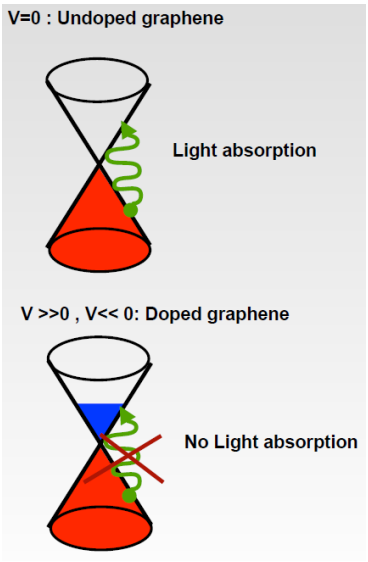


Figure 3.3: Band diagram graphene

With this in mind, the design can be further optimized by also putting graphene on top of the output waveguides. By adding not only a graphene layer to the MMI, but also to the waveguide outputs, we can reduce the output noise by absorbing the light that got caught in the wrong output. So the graphene basically has two major functions in the MMI. On the one hand as an Electro-Optic Modulator(EOM): the graphene over the MMI is used to switch between output states, by a change in $\mathbb{R}e[n_{eff}]$. On the other hand it behaves as an electro-absorber (EA): the layers of graphene over the output waveguides, which can be controlled by different voltages, are used to absorb the excess light. The absorption of graphene is related to $\mathbb{I}m[n_{eff}]$ and can be modified by the gate voltage.

To relate the absorption level to the gate voltage applied over the GOS structure we express the latter as function of the carrier density $n_s$ in the graphene film [28]:

$$V = -V_0 + \frac{d_{ox}e}{\varepsilon_{ox}} \cdot n_s \tag{3.4}$$

with $V_0$ the offset voltage originating from the natural doping in a real graphene sheet and $\varepsilon_{ox}$ the dielectric constant of the oxide layer [25]. Because the carrier density $n_s$ is then directly related to the Fermi level of graphene, which in turn, with the famous Kubo formulas [14, 29], is related to the real and imaginary refractive index and thus absorption. I will not put the formulas here, because they are lengthy, require explanation of a lot of variables and will add nothing

more to the story, but they can be readily found .

Summarizing, adding this layer onto the output waveguides will not increase the losses on the useful signal, while it can perfectly annihilate an unwanted signal, also by only switching the Fermi level between 0 [eV] and 0.52 [eV] (turning on or off a voltage between roughly 0 [V] and 4 [V], depending on the graphene quality and oxide thickness). For a graphene quality leading to a scattering time $scat_T = 100fs$ and an $Al_2O_3$ dielectric layer with a thickness of 10 nm on a Silicon on silica single mode waveguide, we get following results in *COMSOL* for the TM mode(table 3.1):

Table 3.1: graphene as EAM: losses

| $losses\left[\frac{dB}{\mu m}\right]$ | 0 [eV] | 0.52[eV] |
|---|---|---|
| $Si-SiO_2$ | 0.0955 | 0.0032 |

As an extra visualization, the absorption was simulated for different gate voltages for both TE and TM fundamental modes for the standard design in Figure 3.1 with oxide thicknesses of 10 nm and MMI dimensions: 220 nm x 4000 nm. The results can be seen in Figure 3.4.
Because the graphene Fermi potential and the voltage across it are linked through the height of the oxide layer, I get for the Fermi levels 0.52 [eV] and 1.1636 [eV], for an applied voltage of 4V to 20V, because I consistently use oxide heights of 10 nm(The results can be found in section 4.7).

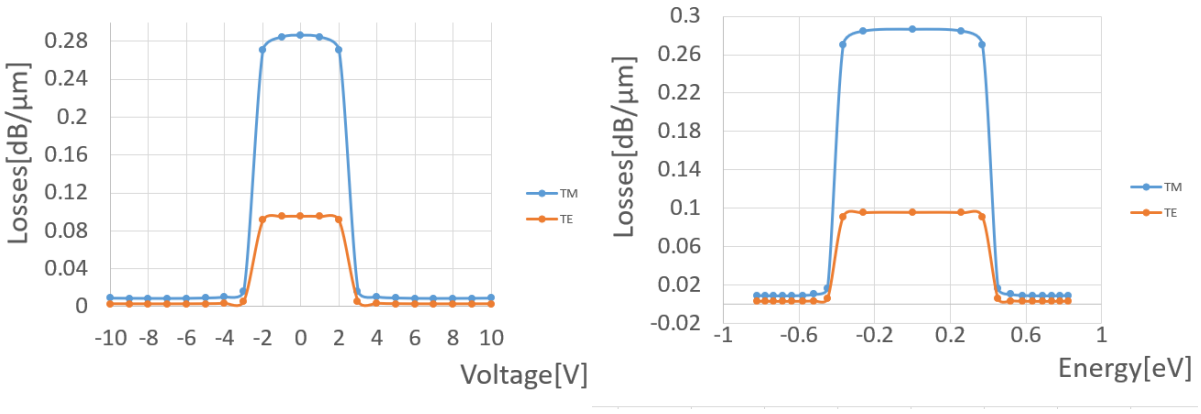


Figure 3.4: TM and TE mode absorption for oxide thickness $d_{ox}$ = 10 nm and $V_0$= 0 V expressed in voltages (left) and Fermi level potential (right)

## 3.3 Dimensions

In the following sections, the dimensions are discussed for a $Si$ on $SiO_2$ MMI. The dimensions will of course change when using different materials. I pick this however as a reference and I will explicitly note the different dimensions when using other materials.

### 3.3.1 In- and output waveguides

The dimensions of the monomode input waveguide are calculated using the 'Effective index'-method(appendix A) near cut-off [30, 31], with the normalized frequency or *"V-parameter"* [32, 33]:

$$V = k_0 \cdot \left( n_r^2 - n_c^2 \right)^{0.5} * d \tag{3.5}$$

where $d$ is the height of the rectangular waveguide.
The number of guided TM modes can be calculated from equation [25]:

$$M = 1 + Int\left[ \frac{1}{\pi}(V - atan(\sqrt{(}a_{TM}) \right] \tag{3.6}$$

In this equation Int[...] means the integer part of the argument. Furthermore $a_{TM}$ is defined as $\frac{n_{cl1}^2 - n_{cl2}^2}{n_{core}^2 - n_{cl1}^2}$ and is just 0 for a symmetrical waveguide.

Therefore, the biggest height one can have that supports only 1 TE or TM mode is when $M < 2$ in equation (3.6), which yields a waveguide height $d = 220nm$ for a wavelength of 1550 nm.

We would like the single mode waveguide to be as large as possible, because then more light is confined in the core and more power can be transmitted across the waveguide with consequently less losses upon propagation. Standard values are in the range [400,500] nm. I picked the smallest -400 nm- width because the wider I make these waveguides, the wider the eventual MMI will be (discussed in section 3.2).

### 3.3.2 MMI and coating dimensions

Firstly, in height, the MMI should remain the same as the input and output waveguides to maintain single mode behaviour, being a 220 nm height.

Secondly, the width of the MMI dictates how many transversal modes there may exist. The MMI should be at least 1200$nm$ wide, as this is the width of the 2 output ports combined with a gap between the two ports of also 400 nm. This puts an absolute lower boundary on the width of the MMI.
The reason for picking the gap 400 nm is because there are 2 adjacent evanescent fields that are reduced in power by a factor $e$ after a distance (y-direction) of roughly $\frac{\lambda_0}{10}$=155nm. Because there are two adjacent fields, this adds up to 310 nm and then I add a small margin of 90 nm because it adds extra reduction in coupling, increasing the switching efficiency and lastly the uniformity of the layers is more esthetically pleasing.
In my actual models I go up to a gap of 600 nm, where the coupling becomes unnoticeably low.

We want the width of the MMI to be as small as possible, because the beating length between the modes ($L_\pi$) scales quadratically with the width of the MMI. However, if the width is too small, there's a lot of crosstalk between the output waveguides and for very small gaps between the output waveguides, the multimode beating just continues in the output waveguides, as can be seen in Figure 3.5. This result was obtained for an MMI width of 2 $\mu m$. From this point onwards, I took a standard width of 4$\mu m$ for all the MMI designs. In hindsight this was not the best idea as it has a detrimental effect on the results and the effect of coupling only becomes prominent after long lengths of propagation and a small constant gap between the output waveguides (and an be remedied in better ways such as bending the output waveguides). The final result does again have a 2$\mu m$ MMI width (and a 600 nm gap).

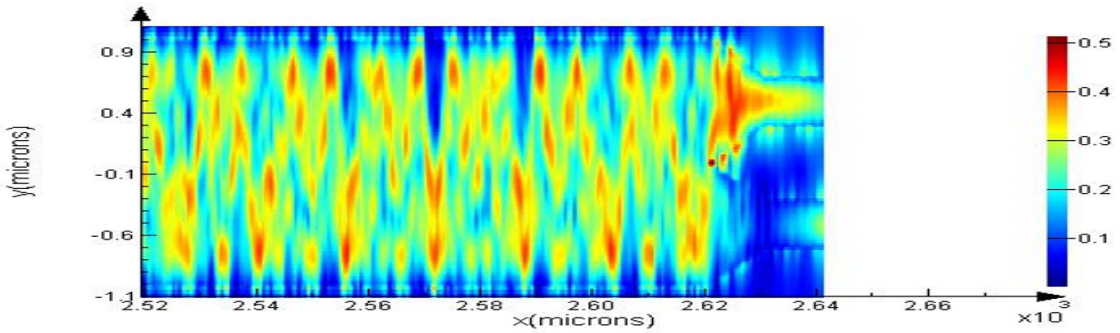


Figure 3.5: unwanted beating in output waveguides

### 3.3.3 Dielectric covers

The dielectric layers on top of the MMI are chosen in such a way that they optimize the coupling of the fundamental TM mode to the graphene, assuming a TM mode fundamental input. For this, a small layer of $SiO_2$, that has a fairly low refractive index, is deposited on top of the waveguide as an isolation from the waveguide. On top of this layer of $SiO_2$, we put a layer of $Al_2O_3$ that is sandwiched between 2 sheets of graphene. As $Al_2O_3$ has a higher refractive index than $SiO_2$, we confine the light better in this layer in intimate contact with graphene on both sides in order to optimize the coupling. As this was my standard design, I did not check the improvement with respect to for instance 2 $Al_2O_3$ layers, but this could have been done.

For the dimensions of the dielectric layers in close contact with graphene, I took as a reference a similar waveguiding structure but with a SLG instead of a DLG [16]. The layers should have a thickness between 1 nm and 30 nm and not more, because the thicker this dielectric, the further we go away from the TM Electrical field maximum and the higher the required voltages to switch.
Because thin dielectric layers act as capacitors, reducing the oxide height, decreases the possible modulation speed($\tau = R/cdotC$). We are however not interested in very fast modulation speeds, as we don't wish to modulate a signal, but rather multiplex (or switch) it.
Hence we could use thinner oxide layers, which increases the coupling to graphene and thus reduces the required operation voltages.
In this reasoning, we could go down to 1 nm height for the oxide (or as small as possible) if this is technologically possible and we find a suiting dielectric.

The reason I still opt for a dielectric layer of around 10 nm is the following: as the spacing between the capacitor plates, or equivalently, the oxide thickness is reduced, the breakdown voltage of the capacitor will be lower, but the coupling will be higher to the graphene. Thus I believe it is best to maintain a dielectric thickness for which we know we can produce it reliably and with good quality, rather than a thin dielectric layer that might have a lot lower breakdown voltage due to fabrication errors.
Both $Al_2O_3$ and $SiO_2$ have very high breakdown voltages(see table 3.2) and can be deposited in a qualitative manner for a height of 10 nm.

The capacitance of one such oxide layer can be written as:

$$C = \frac{\varepsilon_0 \varepsilon_r A}{d} \tag{3.7}$$

with $\varepsilon$ the dielectric constant of the used oxide, $A$ the surface area and d the oxide height.

The break down voltage is material dependent and from 'trustworthy' sources on the Internet I gathered these break down voltages [34] in table 3.2:

Table 3.2: Breakdown voltages

| nothing | $Al_2O_3$ | $SiO_2$ |
|---|---|---|
| $BDV\left[\frac{V}{nm}\right]$ | $0.5to3$ | 1 - 2 |

## 3.4 Materials

I chose the reference setup as shown in Figure 3.1. The reason I picked these materials is because a similar prototype has already been made with and tested for a waveguide with this structure, but with different materials[16, 27]. Because an MMI profits most from higher index contrast and *Si* has a very big refractive index, this was an obvious choice for a standard design. In section 3.5.1, I also explore a somewhat different design and use different materials to see which setup performs best.

Si and $SiO_2$ were chosen as respectively core and cladding of the waveguiding structure because Si photonics is CMOS compatible, nontoxic and due to high index of refraction ratio, compact [22].

$LiNbO_3$, $As_2S_3$ and SiN waveguides as a substitute for Si are tested firstly because they have good transparency in the IR region.

Furthermore, $LiNbO_3$ has electro-optical properties and flexible tuning capabilities. It can provide as a low-loss channel waveguide[35].

For $As_2S_3$, the reason of choice is that it is a chalcogenide glass with a large index contrast that enables tight mode confinement and low propagation loss. It can also be fabricated using CMOS compatible technology [35]. This was in the end not modeled due to time shortness and its result should be in line with the other materials, being somewhat suboptimal with respect to *Si*.

SiN does the same job as Si, but it has a lot lower refractive index. As such it will increase the dimensions of integrated structures, which makes it a worse choice. However, a higher refractive index contrast makes the waveguide more prone to scattering losses due to nm-scale roughness of the sidewalls of the waveguide. The effective refractive index in SiN waveguides is also less sensitive to the waveguide width due to the lower index contrast [36].

Lastly, I thought of using zinc oxide(ZnO), as it has good waveguiding and insulating properties, so it may be used as a replacement for the waveguide. It cannot be used as the dielectric layer between the sheets of graphene, because its breakdown voltage is too low by 2 orders of magnitude (the BDV goes up to 1.6 kV/mm).

My idea was to test another dielectric layer on graphene, but I cannot find any other dielectric layers that can withstand breakdown voltages up to $2V/nm$.

## 3.5 Coating graphene method

In order to achieve small contact resistance between graphene and metal electrodes (usually Au or Ni) is primordial for reducing losses in graphene-based electro-optic devices. The standard way of making graphene-metal contacts (such as depicted in Figure 3.1), in general have high resistance since graphene lacks vertical surface bonding sites [27]. Graphene's modulating speed is in fact not limited by the carrier transport, but is mostly restricted by the parasitic capacitive effects formed by the graphene-dielectric-graphene stack, graphene-sheet resistance, and graphene-metal contact resistance. Usually, in order to electrically connect the metal and graphene, the metal is deposited on graphene's top surface. The metal and graphene interaction in the surface contacts approach occurs perpendicularly to the graphene molecular 2D plane. Since graphene lacks vertical surface bonding sites, surface contacts are fundamentally incapable of maximizing metal and graphene interaction due to weak orbital hybridization and chemical bonding with the metal [27].

### 3.5.1 Coupling-enhancing waveguide design

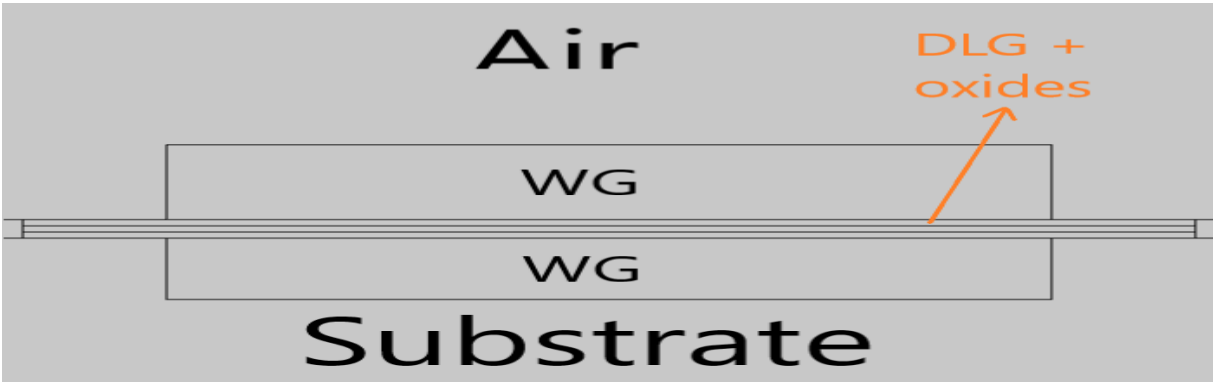


Figure 3.6: cross section of an exotic ridge MMI

Additionally, I made a design of which I'm not sure it can be easily fabricated, but if it is possible, then it shows a big increase in coupling to graphene for the TE modes. Actually the design is completely the same as the standard design shown in Figure3.1, but where the waveguide is not made its full height deep inside the substrate, but only a fraction of it. The rest could then be deposited on top of the top graphene layer as shown in Figure3.6. The modes will course be somewhat distorted by this addition of oxide and graphene in the middle of the waveguide.
For this design, we want to track the TE modes, rather than the TM modes, because they have their Electrical field maximum in the center of the waveguide (both above and below the graphene) and as such, the TE modes commonly have a lot better overlap with the graphene than the TM modes. The results of these designs can be found in section 4.2.

### 3.5.2 Exotic graphene design

Firstly I note that I also use a double layer of graphene (DLG) in the following models (Figure 3.7). The reason is that a double layer graphene has been shown to be experimentally feasible [27] and adding more or less layers just adds the effects of a single layer, because the layers don't interact with one another.

The two designs that were tested and optimized are shown in Figure 3.7.
The idea behind these designs is explained as follows: the MMI coupling length is defined by the beating of the two lowest order modes. As such, the concept seemed promising to get as much coupling to the fundamental mode, while ef-

fecting the first order mode as little as possible or vice versa.
By placing the layer of graphene not over the entire MMI structure, but mostly where either the fundamental or the first mode propagate, we got much better (shorter) results for the required MMI length.

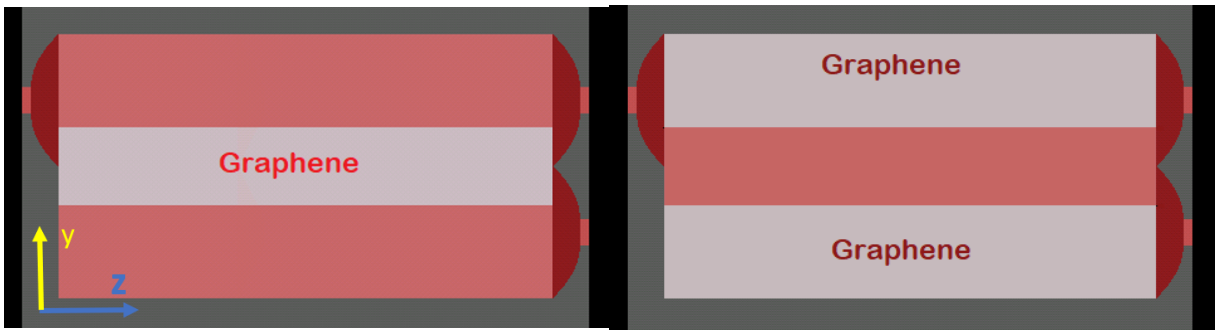


Figure 3.7: left: Graphene deposited over fundamental mode; right: Graphene deposited over first order mode

These designs drastically increase the device's performance such that they reduce the required length down to hundreds of $\mu m$s (results in chapter 4).

## 3.6 Novel MMI design

Virtually all of the tweaks and improvements in the model are there most importantly to decrease losses. This is why we wish to decrease length of the MMI, coated with graphene, because, as low as the losses may be in graphene, they are still very strong when we propagate over several millimeters inside it.

Because a reduction in the coupling length of an MMI would decrease the necessary MMI length I believe it is a good idea to test a more exotic 'Butterfly' design of an MMI as shown in Figure 3.8. Furthermore, as the in- and output waveguides are angled with respect to the propagation direction, there should be less crosstalk between the output waveguides. Theoretical results on this specific MMI design, claim that the coupling length can be reduced by 60% [20].

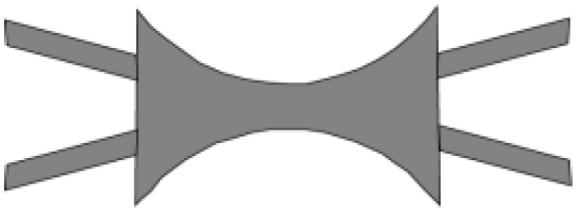

Figure 3.8: Butterfly configuration of an MMI [20]

Firstly, the reason we would like to make the MMI as small as possible is because in a less wide MMI, the beat length $L_\pi$ is smaller. This can be verified in equation (2.2).

Secondly, the reason we would like the MMI to be as wide as possible, is because the output waveguides are so closely spaced that the light trapped inside the output waveguides still interferes and increasing the width of the MMI allows for more spacing between the output waveguides.

As a conclusion, the necessity for a larger width only poses itself at the output of the MMI, and the thinner MMI is more beneficial upon propagation. As such this butterfly-design concept seemed promising.

From results obtained with *Lumerical*, the speeding up of the coupling length $L_\pi$ around the smaller core of the MMI can be visually perceived in Figure 3.9.

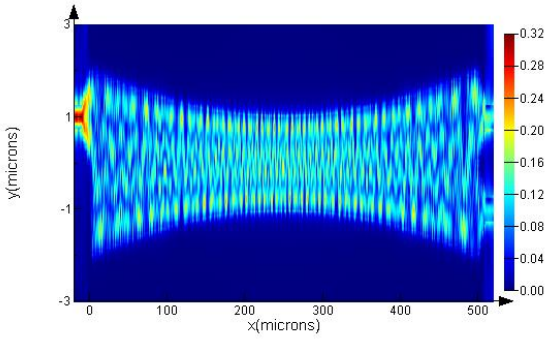


Figure 3.9: coupling length reduction

However, we do see that the field profile gets distorted and spread out a lot in space in the butterfly model, which will make the switching action more difficult. As such, I didn't implement this on further MMI designs.

## 3.7 Difficulties in modelling graphene

As Graphene is not present as a material in the *COMSOL* library, a first idea was to model the MMI in *COMSOL*, both in 3D as in 2D and manually changing the refractive index for the different cases of different doping levels in graphene. This did not take into account the losses that are present inside the material. However, for graphene, the losses are very small in the regions where the refractive index changes strongly, so we thought this to be a good plan.

In order to reduce the very time-consuming 3D calculations in *COMSOL*, a 2D longitudinal cross-section was built and tested, but the results were wrongly interpreted, as verified a lot later by *Lumerical*. It is such that in the 2D simulations, the third dimension is assumed infinitely long and as such, some modes that were showing guiding in 2D, actually were below cut-off in 3D.

Because the wrongly assumed correct dimensions were unrealistically small, the model for the MMI had to be updated to larger dimensions, but as the necessary length of the MMI scales quadratically with the width, the model suddenly changed from a $\mu m$-order component (same order as similar components with the same functionality) to a *mm*-order component. Now, the losses after propagating several millimeters in graphene are not negligible at all, so even these relatively small losses lead to total absorption of the signal inside the MMI. This is the primary reason why different designs had to be explored for both graphene as for the MMI to get feasible results.

# Chapter 4

# Theoretical results on MMI coated with graphene

It is important to note that this simulation model, using the surface current model [15], corresponding with a certain equivalent thickness of graphene, leads to similar results as was verified through direct comparison in this paper [16] for a very similar structure.

To model the influence of graphene on the MMI, we represent it as a change in refractive index.
Lastly, I also wished to include thermal properties in the model, because temperatures are supposed to increase during operation and this will have its effect on the refractive index. I however abandoned this track as I was told this wouldn't influence the results too much.

## 4.1 Standard design results

In the Figure below (4.1), the standard design is shown.

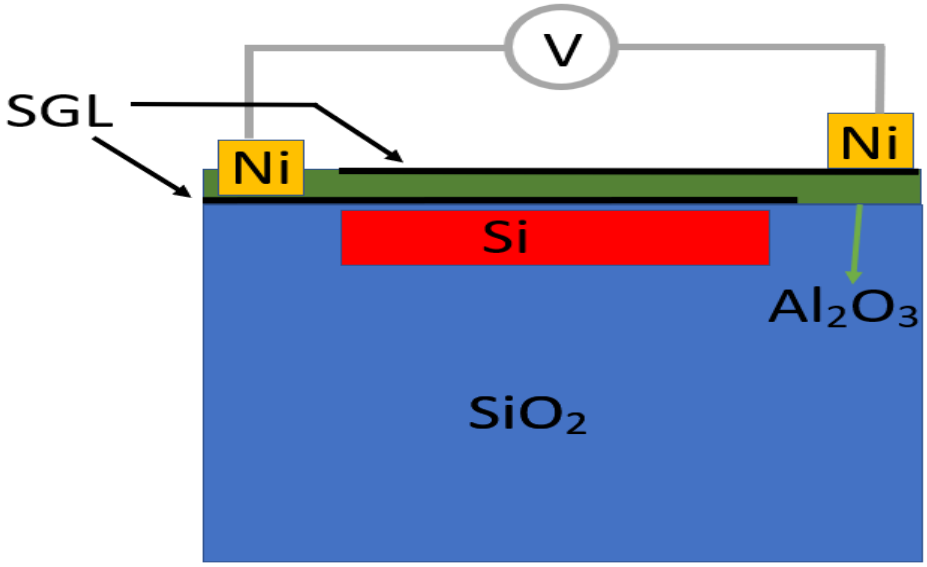


Figure 4.1

Because this design gives a final MMI length of around 9 mm, even using the fundamental TM mode (Figure 4.2), that does not allow this component to be used as a switch due to the losses.

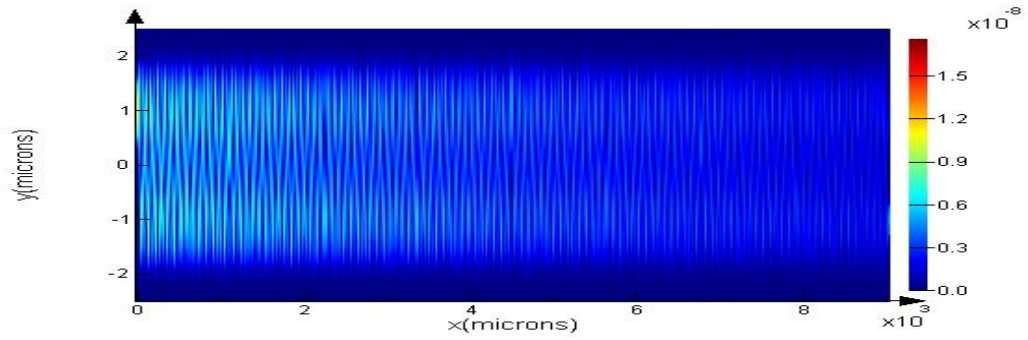


Figure 4.2: Losses completely destroy the signal after propagation over 9mm in the MMI coated with graphene

This is why I will directly pass to the results of improvements to the design.

The final length of the MMI depends virtually only on two parameters: the effective coupling we get with the graphene sheet and the effective width of the MMI. As such, I tested various designs of MMI's (having different coupling to graphene) and variations on the MMI width. In sections 4.2 and 4.3, I check the variations in coupling efficiency and in section 4.6 I explore the variation on the width.

## 4.2 Results on novel WG design

A novel design idea was to deposit a part of the waveguide on top and a part below the graphene sheets that are embedded in dielectric layers as in Figure 3.6. I compare results for a few of these designs for some different waveguiding materials in the following sections. Changing a material of course means that the dimensions will be different to ensure proper waveguiding. For every different material, I will thus note which dimensions I use.

To clarify my designs, I use a parameter R that stands for the ratio of the waveguide that is on top of the graphene. For instance, a ratio of 0.7 means that 70% of the waveguide's height is on top of the "$SiO_2$-graphene-$Al_2O_3$-graphene"- structure.
To display correctly the effect that graphene has on the MMI, I should either show the effective refractive index of all propagating modes separately, either show the effective index of the resulting structure.

For qualitative results on the MMI where graphene is coated over the entire structure, the influence of graphene can be shown by displaying the refractive index of only the fundamental mode, because this is a lot less time consuming and I didn't have much time in the end.

For results where graphene is not deposited over the entire structure, this assumption is definitely not valid anymore and I show results based on the effective index of the two most impactful modes or all the modes.

For different materials as waveguide, I show different ratios R. For R=0, I show the effect of both the fundamental TE mode and TM mode, because it gives a references of the improvement that the new design has. For other ratios I leave out the TM mode as it has nearly no spacial overlap with graphene in this structure and thus has nearly no coupling.

### 4.2.1 Si on SiO2

For a waveguide height $h = 220nm$ and width $W_M = 4um$:
Comparison for the best ratios of the fundamental mode:

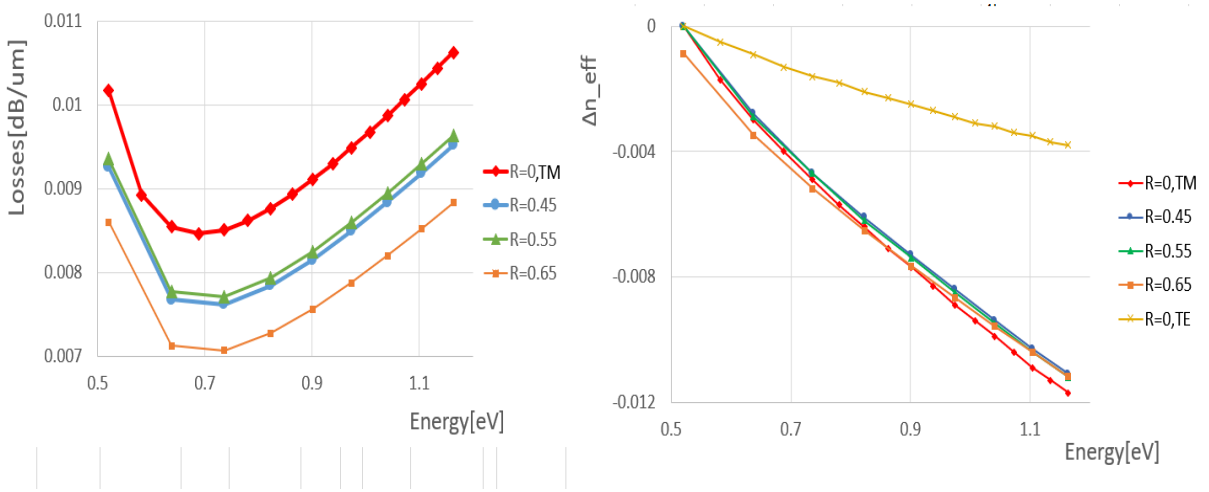


Figure 4.3: losses and $\Delta n_{eff}$ for the designs with R=0, 0.45, 0.55 and 0.65 vs the Fermi level of graphene.

From Figure 4.3, we see in the losses on the left that TE modes don't couple as well to graphene as the TM mode for ratio R=0. However for the ratio R=0.55, the TE mode relatively closely approximates the coupling from the TM mode. I left out the TE mode for R=0 in the left side for visualization purposes. On the right side I added the coupling (now expressed in terms of refractive index) of the TE mode with ratio R=0 to compare the relative improvement of the new design. I just add for clarification that if a mode has higher absorption, then it must be because the coupling with graphene is better, because there are no other losses included in the model[1]. Values for TM mode for R=0 and TE mode for the best ratio (R=0.55) are put in following table:

Table 4.1: Si on $SiO_2$ change in $\Delta n_{eff}$

| potential[eV] | $\mathbb{R}e(n_{eff})$, TM0 | $\mathbb{R}e(n_{eff})$, TM1 | $\mathbb{R}e(n_{eff})$, TE0 | $\mathbb{R}e(n_{eff})$, TE1 |
|---|---|---|---|---|
| 0.5203 | 1.9248 | 1.8971 | 2.707 | 2.6863 |
| 1.1636 | 1.9137 | 1.8863 | 2.6958 | 2.6750 |

I explicitly add the refractive indices in the table, because this information gets lost when plotting the change in refractive index.
The reason that the TM mode still performs better than the TE mode is that the mode profile of the TM mode is very confined on at the interface of graphene and the dielectrics and thus the Electrical field can couple more strongly. The TE modes have their energy more spread out over the entire waveguide and as such have less coupling. The difference can be seen in Figure 4.4.

[1] I model $SiO_2$ in *COMSOL* with the refractive index $n = 3.48 + j * 10^(-7)$

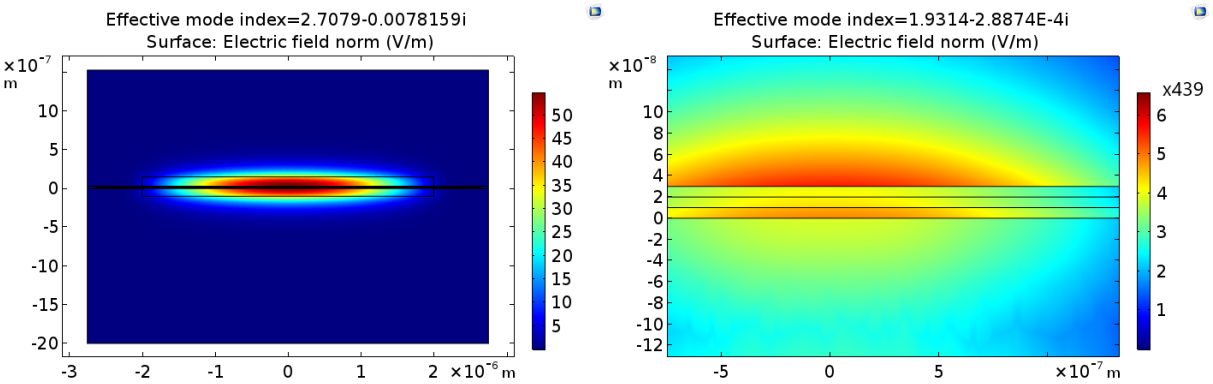


Figure 4.4: I will update the scaling factor later; but the Field intensity is larger at graphene's surface for TM

### 4.2.2 LiNbO3 on SiO2

For a waveguide height $h = 450nm$ and width $W_M = 4um$: Comparison for the best ratios of the fundamental mdoes:

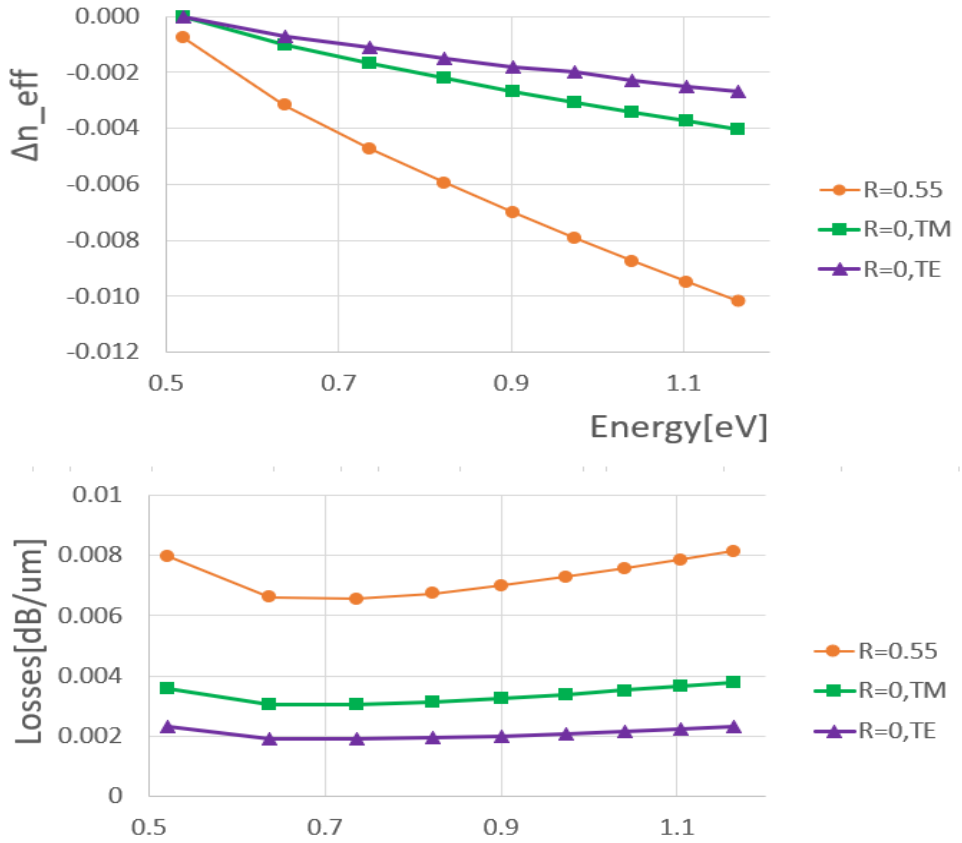


Figure 4.5: losses and $n_{eff}$ for R=0(TE and TM) and the best ratio R=0.55

We see here that the TE mode actually does a better job at changing the refractive index than the TM mode at R=0. Due to the larger dimensions and smaller refractive index contrast with the cladding, the mode profile is more spread out for the fundamental TM mode and as such, the TE mode, which has its maximum at the graphene sheet has a lot better coupling.

The z-cut $LiNbO_3$, that I modeled, is a highly birefringent material and as such, the results for TE and TM cannot just be interpreted without taking this into account. The refractive index difference between $n_e$ and $n_o$ at $\lambda = 1550nm$ is on the order of 0.07. Now, because we insert either TE or TM in the input fibers, all modes lie in the same plane and feel the same refractive index. As such, this will have no effect on the beating pattern itself other than a fixed delay for all modes. As the effect of this anisotropy has a minor effect, I did not explicitly show the results for the two extremes.

### 4.2.3 SiN on SiO2

For a waveguide height $h = 600nm$ and width $W_M = 2um$ of the fundamental modes:

Comparison for the best ratios[3]:

The *SiN* waveguide also has its energy more spread out for the TM mode, just like $LiNbO_3$. As such, the TE mode at R=0.55 has better coupling to graphene. As it has a slightly lower refractive index contrast than $LiNbO_3$ with the cladding, the results are just a bit worse.

[3] I model *SiN* in *COMSOL* with the refractive index $n = 2.016 + j * 3 \cdot 10^{(}-7)$

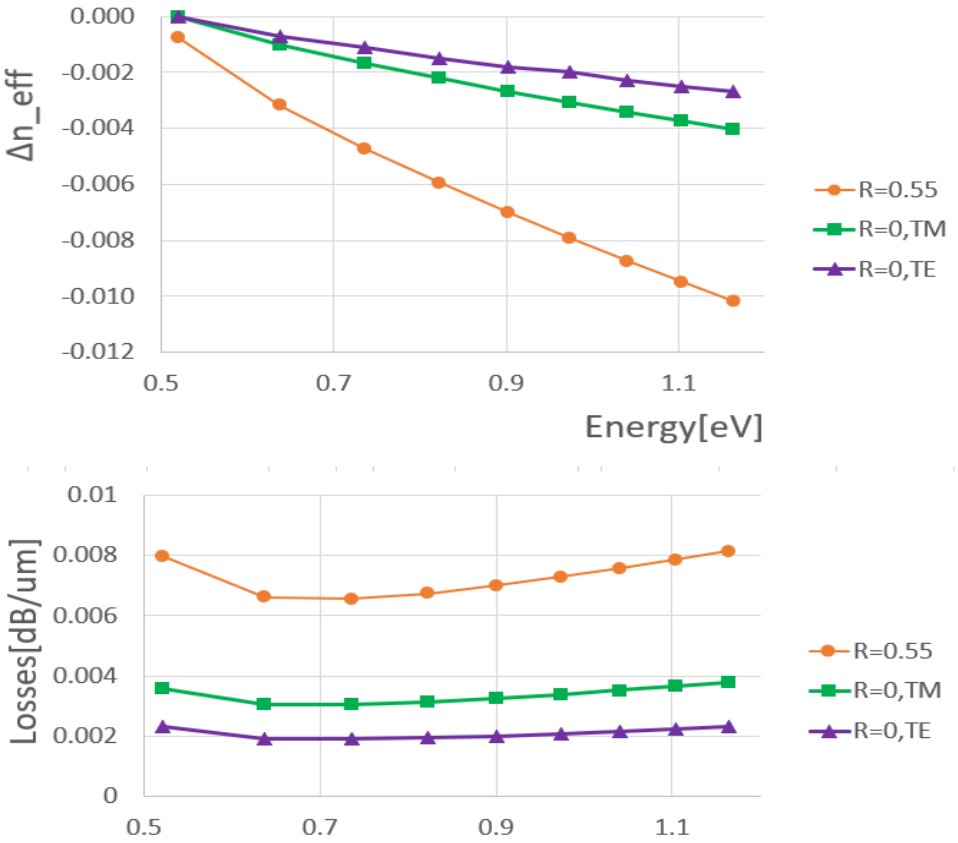


Figure 4.6: losses and $n_{eff}$ for R=0, 0.65, 0.7 and 0.75

The reason why TM modes outperform the TE modes is because of the better spacial overlap with graphene.
As a side-note, the reason that the TM modes have any coupling at all in this case is peculiar, because the E-field polarization orthogonal to the graphene plane should show no or very small interaction. The reason that the TM modes still couple to graphene is because of the hybrid modes that have a component in a direction in the plane of graphene.

## 4.3 Novel graphene design

The two designs under test (Figure 4.7) have been optimized to show the best coupling to either the fundamental or the first order mode (respectively left and right design) by searching the ideal widths of (y-direction) the graphene sheets.

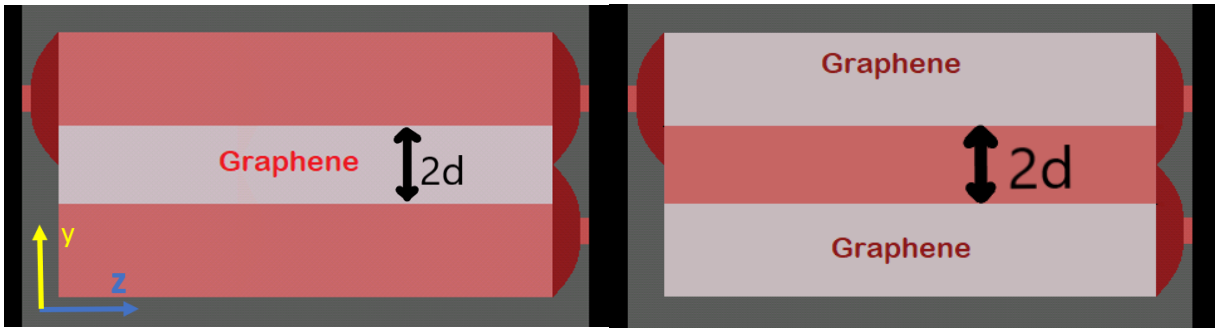


Figure 4.7: left: Graphene deposited over fundamental mode; right: Graphene deposited over first order mode

The performance of the design with the layer of graphene on the sides is shown in Figure 4.8. Here, parameter d equals half the distance between the 2 sheets, measured from the middle of the MMI. We see that the losses increase with increasing d. This is as expected, because there is more graphene with which the light can interact, leading to more losses.

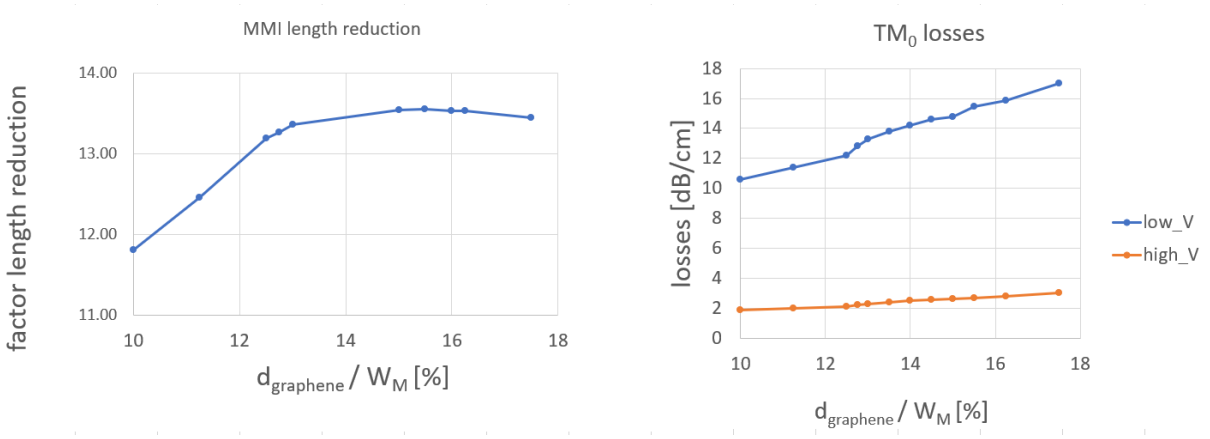


Figure 4.8

The performance of the design with the layer of graphene in the middle is shown in Figure 4.9. Here, parameter d is half the size of the graphene layer in the middle measured from y=0. Here we see the losses decreasing, which is logical, because for decreasing d in this case, there is less overall graphene on the structure.

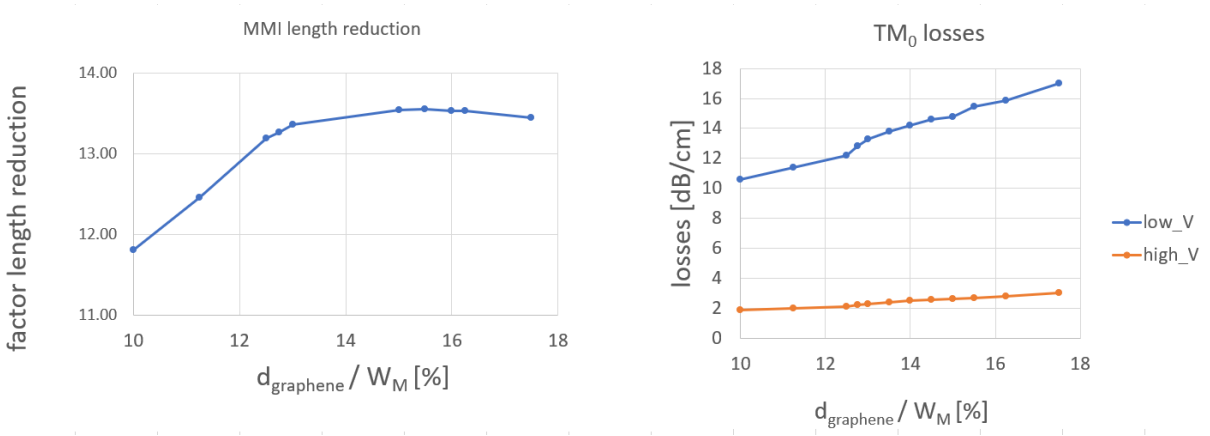


Figure 4.9

The optimal value for both designs I found for d is around $\frac{d}{W_e} = 15\%$ or concretely $d = 0.62\mu m$ for an MMI of $4\mu m$. For this optimal value I show switching behaviour of the 2 designs for an MMI length that has been reduced to around $600 - 700\mu m$(Figures 4.10 and 4.11).

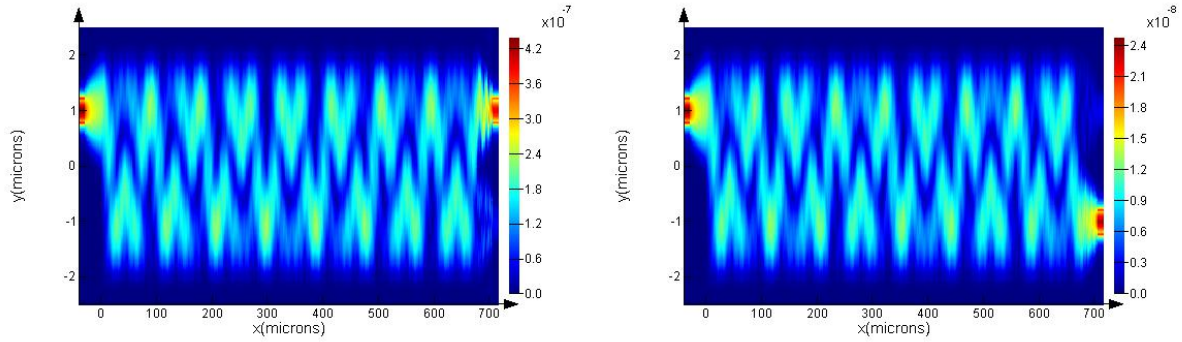


Figure 4.10: middle design; left: Fermi-level=0.520 [eV]; right: Fermi-level=1.1636 [eV]

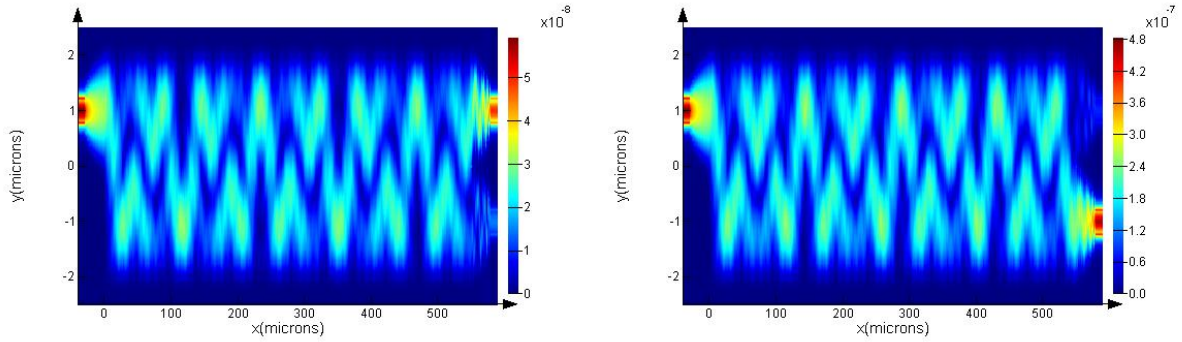


Figure 4.11: split design; left: Fermi-level=0.520 [eV]; right: Fermi-level=1.1636 [eV]

It seems that the split-layer concept does a slightly better job than the design with graphene in the middle. The difference between the two designs is however negligible with respect to the reduction in MMI length that they both bring to the table. With these designs, the component works 13-15 times better.

## 4.4 Best result

Given the fact that *Lumerical* only yields TE-mode propagation profiles (I don't know why), the best result I find is based on TE modes.
Combining the split-layer-graphene concept (section 4.3) on a *Si* on *SiO*2 for a thin MMI with thickness $2\mu m$ and the bi-layer of graphene about the middle of the structure (R=0.55) and changing the Fermi level between $0,52[eV]$ and $1.1636[eV]$ for a fundamental TE mode input, I get a switch that has a length of $139\mu m$. The results can be seen in Figure 4.12.

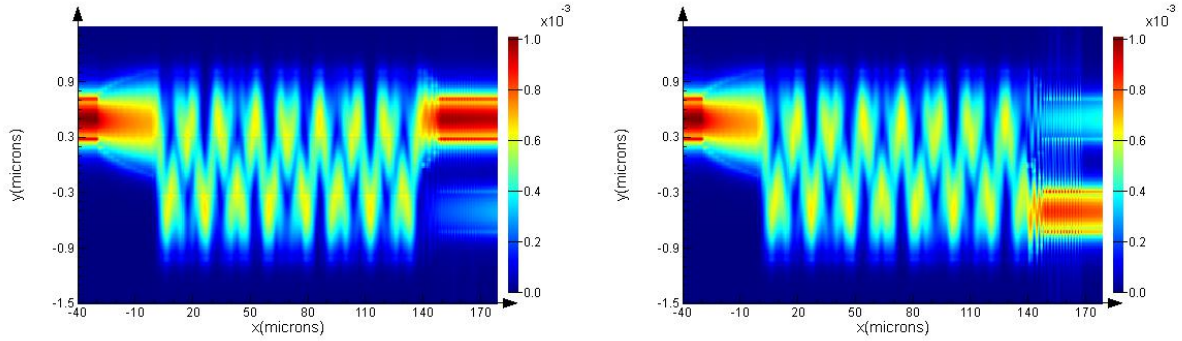


Figure 4.12: split design; left: Fermi-level=1.1636 [eV]; right: Fermi-level=0.52 [eV]

The results for the refractive indices can be found in table 4.2 below.

Table 4.2: best result for TE modes: refractive index and losses

| potential[eV] | $\mathbb{R}e(n_{eff,TE_0})$ | $\mathbb{R}e(n_{eff,TE_1})$ | insertion losses [dB] |
|---|---|---|---|
| 0.5203 | 2.7124 | 2.6280 | 4.75 |
| 1.1636 | 2.7070 | 2.6175 | 0.69 |

To be fair, the switch length shown in this result does not match the length calculated by the formula, but occurs at a lot shorter distance. This is because I found that within the beating profile there are a few instances at which the light mirrors the input, albeit less pronounced or clear.
Calculation of the values in table 4.2 with the formulas described in section 2.2, yields an MMI length:

$$L = 467.6\mu m \tag{4.1}$$

So we get a reduction of a factor 3.33 by picking an intermediate, less optimal solution. However, due to the reduction in length, we skip more than $330\mu m$ of losses at 30dB per cm for $TE_0$.

I also put the values I get for the TM modes which I can't model, but should give a better coupling:

Table 4.3: best result for TM modes: refractive index and losses

| potential[eV] | $\mathbb{R}e(n_{eff,TM_0})$ | $\mathbb{R}e(n_{eff,TM_1})$ | $TM_0$ losses [dB/cm] | $TM_1$ losses [dB/cm] |
|---|---|---|---|---|
| 0.5203 | 1.903 | 1.804 | 16 | 27.5 |
| 1.1636 | 1.898 | 2.97 | 5.2 | 5.63 |

Note that because I can't propagate these TM modes in the structure in

*Lumerical*, I wasn't able to give full insertion losses. Calculation of the values in table 4.3 with the formulas described in section 2.2, yields an MMI length:

$$L = 447.1\mu m \tag{4.2}$$

which is somewhat better than the the result for the TE mode, as expected.

## 4.5 Output cleaning

We see that the splitting is not a perfect 50%-50%, primarily because there is some light that runs away in the other fiber output. This crosstalk can however be nearly completely reduced as discussed in section 3.2. Furthermore, the output power can be easily balanced to get an exact output power in both ports that is equal for the two modes of operation, by adding extra losses to the output that has better transmission of the input signal, so that we have equal power output in both states. In Figures 4.13 and 4.14, one can see both the fractions of the input light that go to the respective output ports, as well as the robustness of the component when the used wavelength is changed. These results were obtained in *Lumerical* for the final design(section 4.4), for TE modes as input.

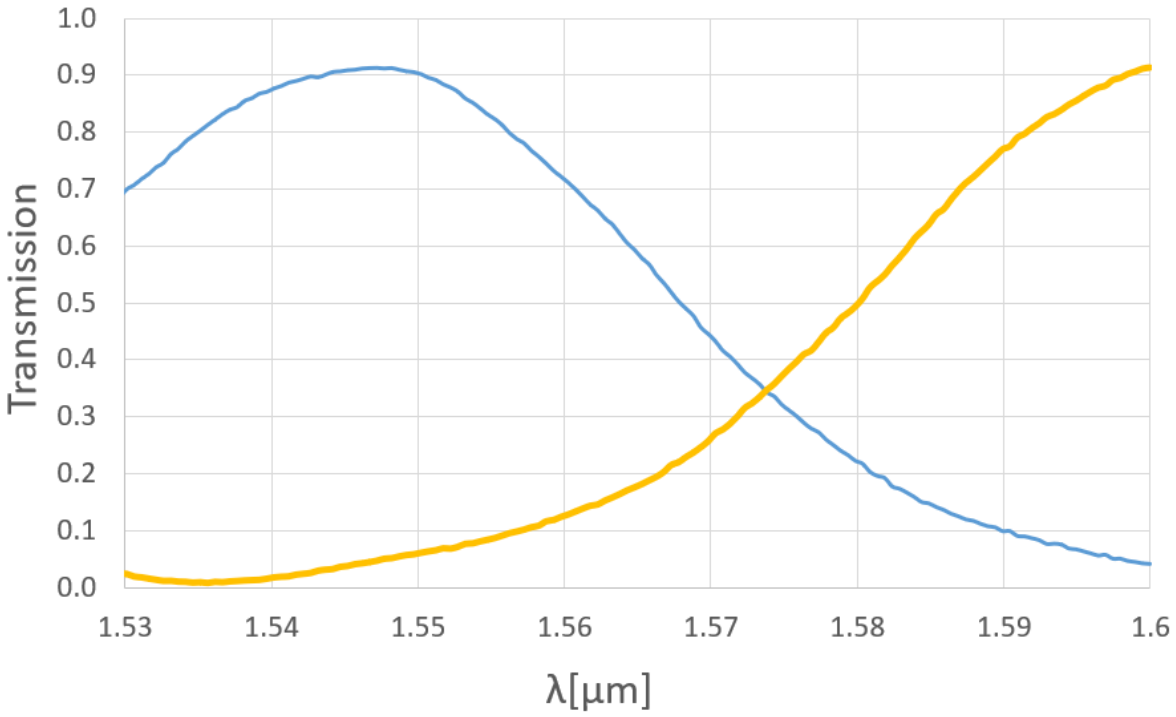


Figure 4.13: Transmission of the input TE light to the upper output waveguide(blue) and the lower output waveguide(yellow) for a graphene Fermi level of 1.1636 [eV] (high voltage) versus wavelength

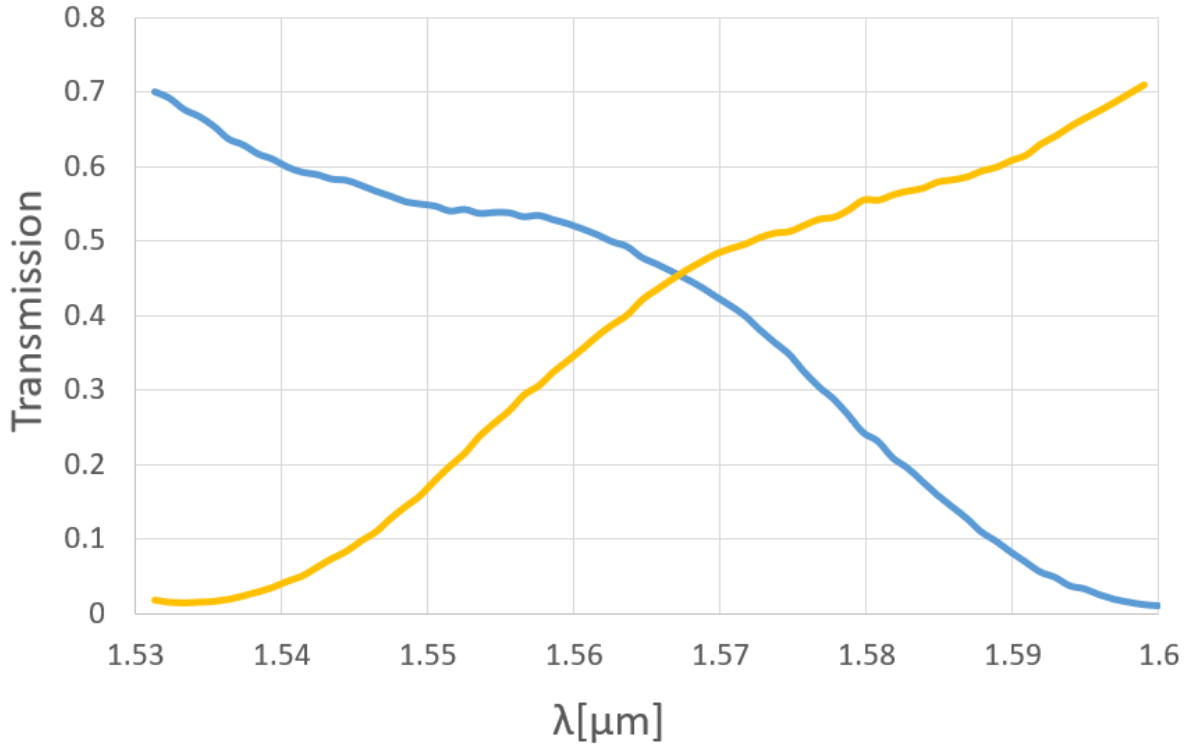


Figure 4.14: Transmission of the input TE light to the lower output waveguide(blue) and the upper output waveguide(yellow) for a graphene Fermi level of 0.52 [eV] (low voltage) versus wavelength

## 4.6 Robustness

Firstly, the robustness of the field profile in the MMI goes down together with beat length $L_\pi$, because when the beating occurs faster, there is a smaller error margin on for instance the exact MMI length. For my standard design with $Si$ on $SiO_2$, with an MMI width varying between 2 and 4 $\mu$ the typical $L_\pi$ varies between roughly 10 and 40 $\mu m$. For an $L_\pi$ of $\approx$ 10 $\mu m$, there is a 1 $\mu m$-margin on the beating profile that gives unnoticeable changes and this scales of course linearly with $L_\pi$.

Secondly, I varied the width of the MMI around 4 $\mu$ with maximum 300 nm to model how geometrical errors on the MMI width influence its length (Figure 4.15).

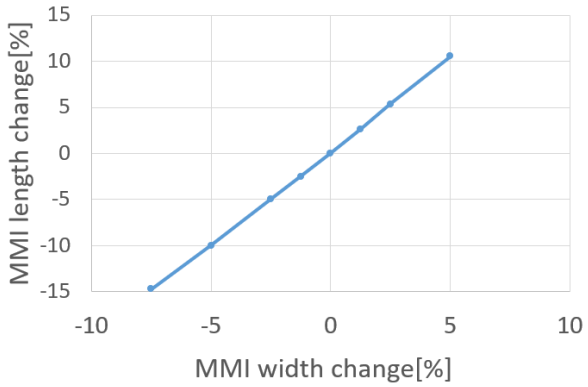


Figure 4.15: effect of small relative width changees to relative length changes

Note that these results are only valid around a width of $4\mu m$ and cannot be extended to other ranges, because they depend on the exact coupling between the modes and graphene and this coupling does not just scale linearly with the width of the MMI.

## 4.7 Dielectric height

Lastly, I tested in *COMSOL* the coupling to graphene for different dielectric layer thicknesses using the Kubo formulas. In Figure 4.16, the results are shown for the change in $n_{eff}$ and losses for a change in the oxide layer thickness of $Al_2O_3$.

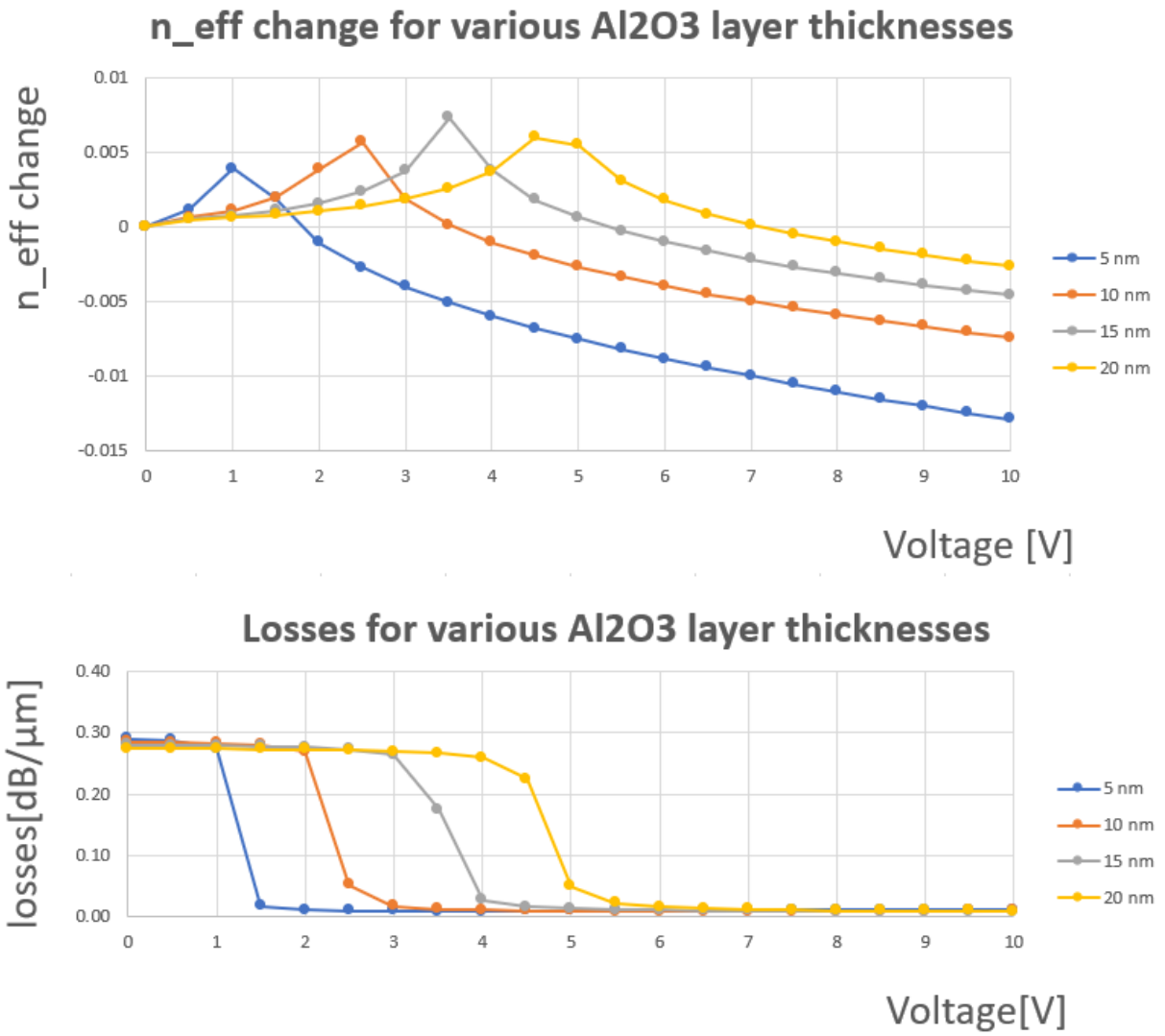


Figure 4.16

Important here to note is that the region in which we are interested, being where the losses are relatively low, shifts up with increasing oxide thicknesses. Thus the required voltages to get a same refractive index shift become bigger. Because there are not a lot of available materials that can be put as dielectric (I didn't even find an alternative to test), the only real variable here is the height of the layer. The layer should be made as small as possible while guaranteeing good quality in order not to get breakdown. As such, I will always use a 10 nm height (see also discussion in section 3.3.3).

# Chapter 5

# Comparison with other graphene-based switches

## 5.1 Mach Zehnder Interferometer

In Figure 5.1, we see how a switch can be built using the principle of a MZI (Mach Zehnder Interferometer).

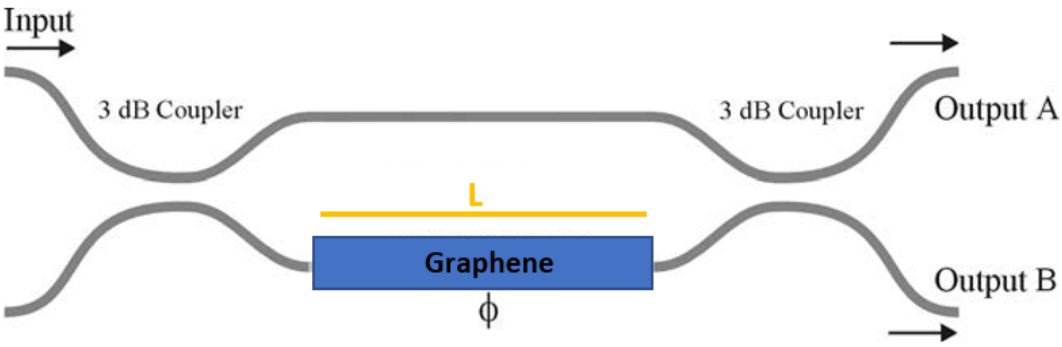


Figure 5.1: Basic MZI scheme

From the theory of a MZI, we find that the power at the output ports (output A and output B) can be written as: [37]

$$P_A = sin^2(\frac{\Delta\Phi}{2}) \tag{5.1}$$

$$P_B = cos^2(\frac{\Delta\Phi}{2}) \tag{5.2}$$

Here, $\Delta\Phi$ is the phase difference of the light in the bottom arm of the MZI with respect to the top arm. This phase modulation is caused by the effective refractive index ($n_{eff}$) change induced by the voltage-controlled graphene.

In order to use this MZI as a switch between the two output ports, as is clear from equations (5.1,5.2), a phase difference of $\pi$ is needed. When we denote the length of the graphene sheet by L (as in Figure 5.1), we may write this phase relation as:

$$exp(j \cdot k_0 \cdot \Delta n_{eff} L) = exp(j\pi) \tag{5.3}$$

In this paper [38] for an MZI-based switch, a value of $\Delta n_{eff} = 0.0026$ is achieved (which is slightly lower than the theoretical maximum coupling I achieve with 2 layers of graphene of $\Delta n_{eff} = 0.007$). Solving this equation for L, yields:

$$L \approx 400 \mu m \tag{5.4}$$

There is thus a propagation over 400 $\mu m$ under graphene to achieve a $\pi$ phase delay of the signal.
The operation of this MZI is similar to the MMI but also in its roots very different. The issue that the MMI has to face with respect to the MZI lies in the fact that the MMI's working principle of mode beating. Putting a voltage across the graphene influences all modes, phase-delaying the beating pattern. For the MZI, there must be a delay in half the period in the end in order to switch, while there is an extra condition for the MMI. The length of the MMI must also be such that this phase delay of half a beating period in the high-voltage-regime occurs, when, in the low-voltage-regime, the beating pattern is at a phase=0. If this condition is not fulfilled, then you get an intermediate value in the beating period that is sent through the output fibers. Luckily enough, for this antisymmetric MMI I designed, there are some intermediate values that closely resemble the phase=0, allowing to make the MMI length shorter than in the strictly theoretical case (section 4.4).

As can be seen in Figure5.2, an extinction ratio of up to 35 dB can be achieved for a voltage of 7.25 V.

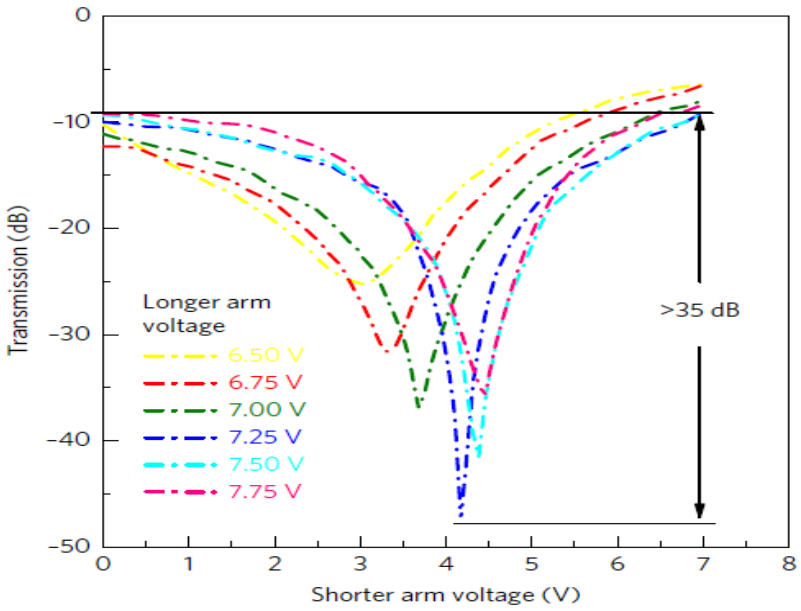


Figure 5.2: Extinction ratio for the MZI-based switch

This MZI shows thus a static modulation depth of 35 dB and modulation efficiency of 0.28 V cm.
The voltage required to switch my proposed MMI is 16V (4V to 20V), with a propagation length of 139$\mu$, yielding 0.22Vcm, which is slightly better than the 0.28 obtained for the MZI switch. The modulation depth, or equivalently in our case, the extinction ratio $\frac{P_{portA}}{P_{portB}}$ can be infinite for the MMI when using active output-cleaning ports (section 4.5), of course at the cost of extra energy consumption.

## 5.2 Microring resonator

A Microring resonator can be used as a switch as is depicted in Figure 5.3.

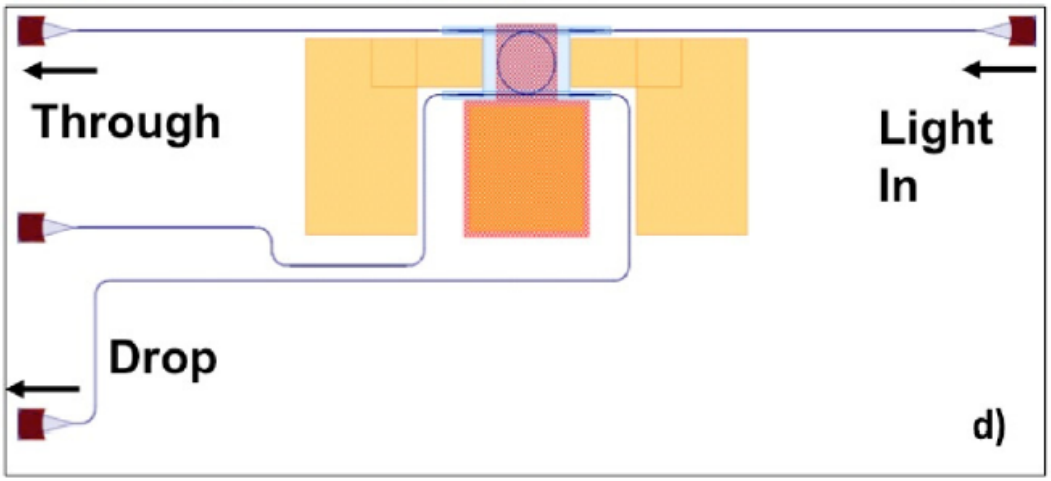


Figure 5.3: Microring coated with graphene setup[39]

The signal goes through the through-port by making the absorption in graphene big enough so that after one round trip, the waves do not interfere in a noticeable way and resonance is suppressed. The signal going through only acquires minimal insertion losses due to coupling from the waveguide into the ring, which is absorbed in the ring path. The other output state is achieved based on the same differential working principle as for the MZI, where a phase difference is obtained in one part of the signal and then rejoined with the other part[39].

In Figure 5.4, the switching quality is displayed from the $25\mu m$-radius microring switch [39].

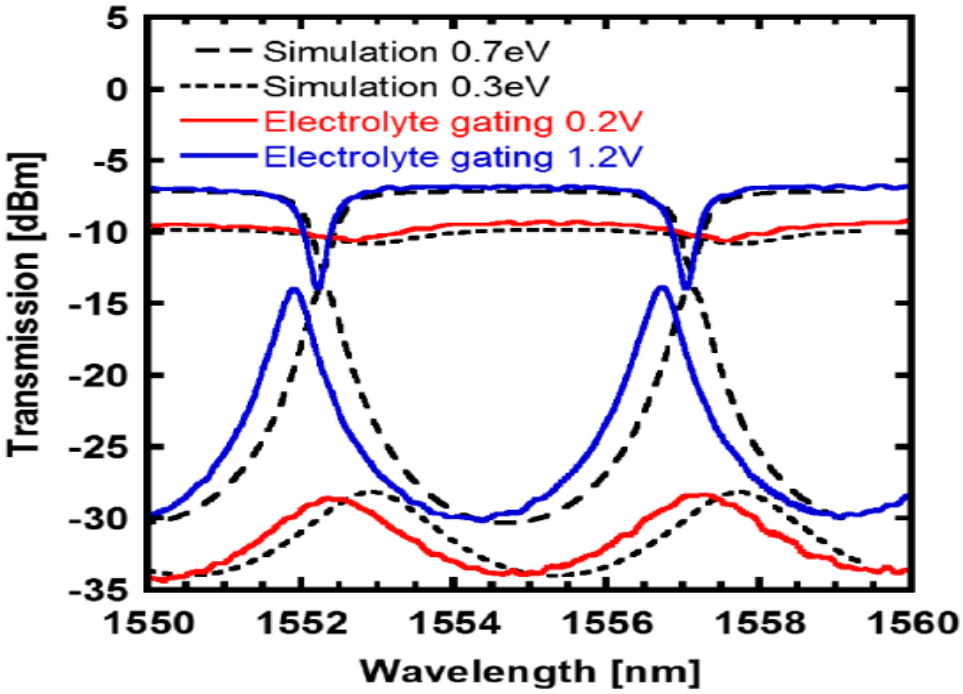


Figure 5.4: Experimental vs simulated results on drop and through transmission spectra[40]

The extinction ratio is around 8dB for a modulation efficiency of 0.28 V cm.

Lastly, worthy of mentioning, from an on-off switch based on surface plasmon polaritons (Figure 5.5), an even higher extinction ratio of 24 dB was achieved[40].

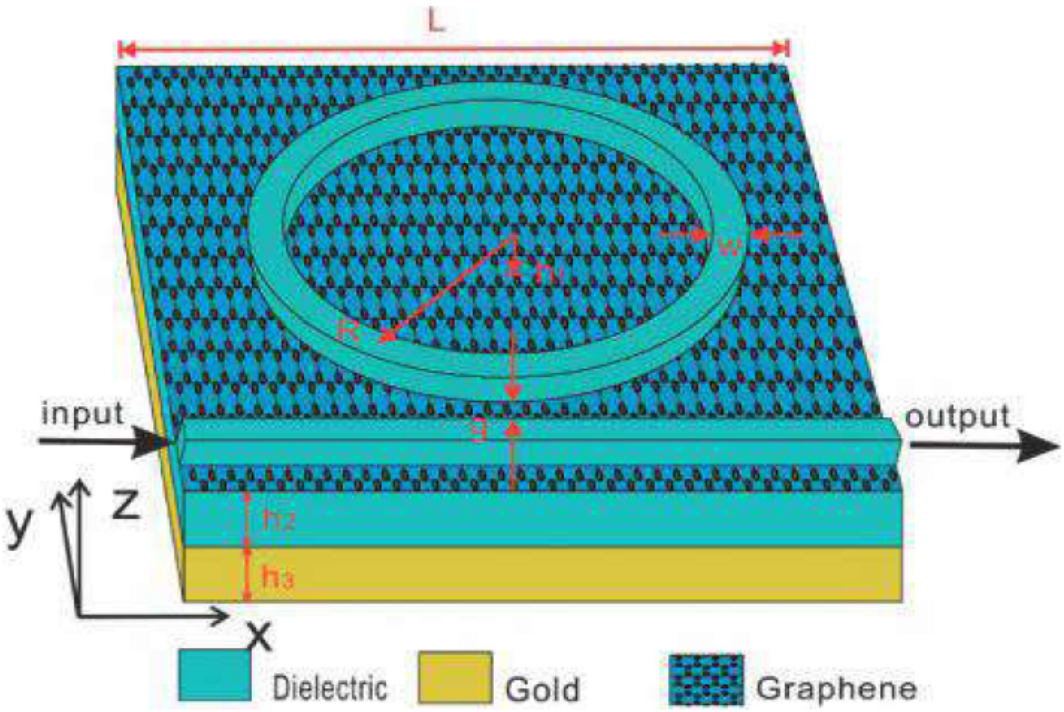


Figure 5.5: Surface plasmon polaritons created on a $Au - SiO_2 - graphene$ interface[40]

## 5.3 Graphene coated directional coupled nanowires

The research 5.6 on this concept goes somewhat out of scope of telecommunication as the experiments were not performed at $1.55\mu m$, but at the somewhat larger 10 $\mu m$. However, I think it is interesting as a comparison for graphene-based switches.
Graphene has a very high third order non-linear coefficient. As such, the non-linear effects that are used for switching, don't require huge amounts of power. When we coat 2 closely spaced nanorods as in Figure 5.6, the system of the 2 rods beats between a fundamental even and odd mode.

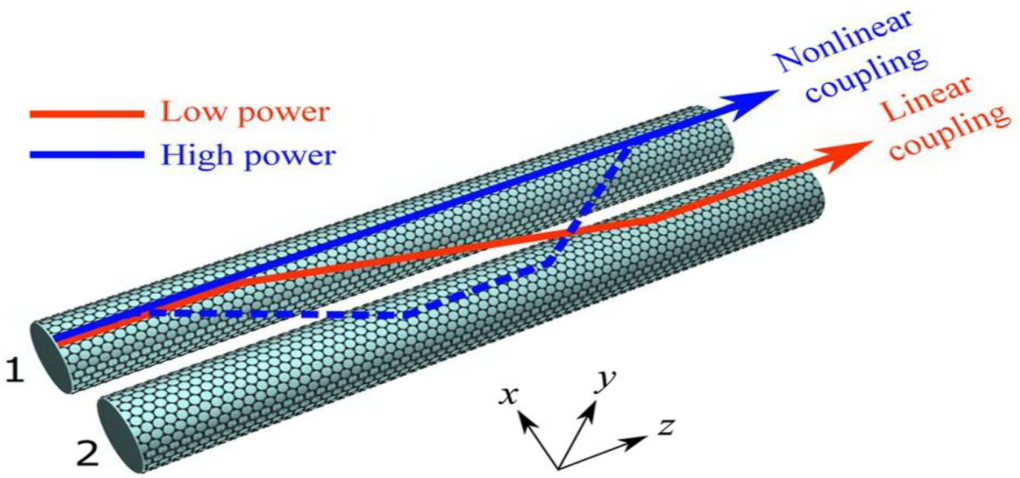


Figure 5.6: Red and blue arrows schematically show the direction of power flow for low and high input power, denoting the linear and nonlinear regimes, respectively.5.6

Concretely, considering a pair of graphene coated nanowires with both a rod radius of 50 nm and distance between the rods d = 150 nm, it was found that this leads to a beat length $L_B$ of 3.52 $\mu m$. At a power $P_0 = 0.01mW$, the system works in the linear regime and all the input power couples to the adjacent rod after a distance $L_B$. With an input power of around $P_1 = 2.9mW$, close to all power remains in the input nanorod, as shown in Figure 5.7. As such, over a distance as short as a few $\mu m$'s, we are able to switch between 2 output ports.

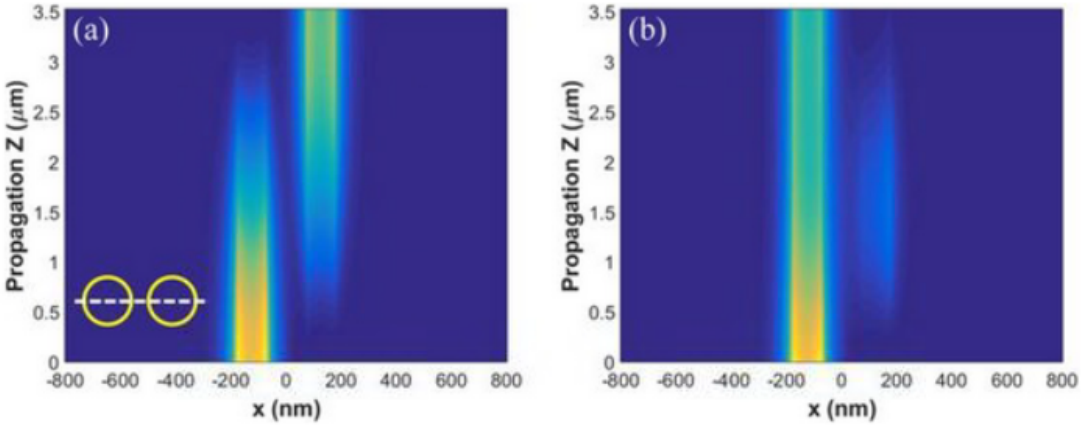


Figure 5.7: Linear coupling(left) versus non-linear coupling (right) to adjacent waveguide.5.6

When the distance between the rods is varied, the distance $L_B$ is changed as well. At a larger $L_B$, the required power can be lower, because of the longer interaction length, but then losses induced by the graphene start overshadowing the switching efficiency. No numbers were stated in the paper, however.

# Chapter 6

# Summary and Future Perspectives

In this thesis I propose a graphene-coated MMI that can perform a 1x2 switching behaviour over 139 $\mu m$ by changing a voltage over 16 V. Furthermore, I explored how this component's performance is altered by among other parameters, using different materials for the waveguide and varying dimensions of a standard GOS design. In this thesis I stick fairly close to what has already been done, to assure that the results I get are feasible or not too far from reality.

The proposed MMI has to deal with a few problems such as putting 2 separate sheets of quality graphene, high quality dielectric layers, tapering the output fibers with a sub-micron gap between ... but when properly done, can get an efficiency close to or better than components that perform similar functions. There are still some improvements that can be made to the model of course.

A first improvement can be made by designing an MMI that reduces the MMI width along propagation, just like the butterfly concept in section 3.8. I abandoned this track because its study was time-consuming and there were more obvious refinements to the model. However, if a proper design can be found that doesn't distort the field profile too much and a proper butterfly-shaped graphene profile can be deposited on top, then this is a definite improvement.

The proposed MMI could definitely be tested in operational bandwidth, influence of increased temperature (due to losses in operation), mechanical stability, sensitivity to polarization and so on.

# Bibliography

[1] F. Zhou and X. Jin. The Mach-Zehnder modulator based on bi-layer graphene-silicon-waveguide. In *2017 16th International Conference on Optical Communications and Networks (ICOCN)*, pages 1–3, August 2017.

[2] G. T. Reed, G. Mashanovich, F. Y. Gardes, and D. J. Thomson. Silicon optical modulators. *Nature Photonics*, 4(8):518–526, August 2010.

[3] F. Xu, S. Das, Y. Gong, Q. Liu, H.-C. Chien, H.-Y. Chiu, J. Wu, and R. Hui. Complex refractive index tunability of graphene at 1550 nm wavelength. *Applied Physics Letters*, 106(3):031109, January 2015.

[4] B. Jalali and S. Fathpour. Silicon photonics. *Journal of Lightwave Technology*, 24(12):4600–4615, Dec 2006.

[5] Different waveguide structures, image found at 3dic.org.

[6] Vilson R. Almeida, Carlos A. Barrios, Roberto R. Panepucci, and Michal Lipson. All-optical control of light on a silicon chip. *Nature*, 431:1081, October 2004.

[7] Scott Jordan. Commercial Tests and Assembly in Silicon Photonics. *Optik & Photonik*, 12(3):31–33.

[8] graphene history, cleverism.com.

[9] Paul Rincon. How sticky tape trick led to Nobel Prize. *BBC News*, October 2010.

[10] Graphene honeycomb structure image, image found at wikipedia.org.

[11] Lecture powerpoint, by Prof. Dr. Ir. Frank Koppens.

[12] Yuan Cao, Valla Fatemi, Shiang Fang, Kenji Watanabe, Takashi Taniguchi, Efthimios Kaxiras, and Pablo Jarillo-Herrero. Unconventional superconductivity in magic-angle graphene superlattices. *Nature*, 556(7699):43–50, April 2018.

[13] Xuesong Li, Weiwei Cai, Jinho An, Seyoung Kim, Junghyo Nah, Dongxing Yang, Richard Piner, Aruna Velamakanni, Inhwa Jung, Emanuel Tutuc, Sanjay K. Banerjee, Luigi Colombo, and Rodney S. Ruoff. Large-Area Synthesis of High-Quality and Uniform Graphene Films on Copper Foils. *Science*, 324(5932):1312–1314, June 2009.

[14] George W. Hanson. Dyadic Green's functions and guided surface waves for a surface conductivity model of graphene. *Journal of Applied Physics*, 103(6):064302, March 2008.

[15] Steven J Koester. Waveguide-Coupled Graphene Optoelectronics, 2013.

[16] Yingtao Hu, Marianna Pantouvaki, Joris Van Campenhout, Steven Brems, Inge Asselberghs, Cedric Huyghebaert, Philippe Absil, and Dries Van Thourhout. Broadband 10 Gb/s operation of graphene electro-absorption modulator on silicon: Broadband 10 Gb/s operation of graphene electro-absorption modulator on silicon. *Laser & Photonics Reviews*, 10(2):307–316, March 2016.

[17] CVD Graphene - Creating Graphene Via Chemical Vapour Deposition.

[18] Kieran Cooney and Frank H. Peters. Analysis of multimode interferometers. *Optics Express*, 24(20):22481, October 2016.

[19] Andres Sosa. Design of Silicon Photonic Multimode Interference couplers, 2012.

[20] MMI Theory and Design. *University of Waseda, Honbun*, page 50.

[21] Optical switching technology comparison: optical MEMS vs. other technologies. 41:S16–S23.

[22] Y DMello, J Skoric, M Hui, E Elfiky, D Patel, and D Plant. Numerical analysis and optimization of a multimode interference polarization beam splitter. *COMSOL conference Boston*, page 20, 2017.

[23] Jesus Perez, Akhilesh Khope, and ECE Department. Multimode interference waveguides. *University of Calefornia, Santa Barbara*, page 14.

[24] MMI coupler with tapered waveguides | Lumerical Knowledge Base.

[25] Course of Microphotonics, UGent.

[26] Teresa Cusati, Gianluca Fiori, Amit Gahoi, Vikram Passi, Max C. Lemme, Alessandro Fortunelli, and Giuseppe Iannaccone. Electrical properties of graphene-metal contacts. *Scientific Reports*, 7(1):5109, July 2017.

[27] Filippo Giubileo and Antonio Di Bartolomeo. The role of contact resistance in graphene field-effect devices. *Progress in Surface Science*, 92(3):143–175, August 2017. arXiv: 1705.04025.

[28] Jacek Gosciniak and Dawn T. H. Tan. Theoretical investigation of graphene-based photonic modulators. *Scientific Reports*, 3(1), December 2013.

[29] V. P. Gusynin, S. G. Sharapov, and J. P. Carbotte. Sum rules for the optical and Hall conductivity in graphene. *Physical Review B*, 75(16):165407, April 2007.

[30] Wei-Chih Wang. Optical Waveguides, Devices and Applications, 2004.

[31] fibre modes, ecee.colorado.edu.

[32] Karsten; Povlsen Jørn Hedegaard Philipp, Hugh Taylor; Rottwitt. *High-Index Contrast Silicon Rich Silicon Nitride Optical Waveguides and Devices*. PhD thesis, Technical University of Denmark, 2004.

[33] RP Photonics, V number.

[34] Y. Q. Wu, H. C. Lin, P. D. Ye, and G. D. Wilk. Current transport and maximum dielectric strength of atomic-layer-deposited ultrathin Al2o3 on GaAs. *Applied Physics Letters*, 90(7):072105, February 2007.

[35] Xin Wang and Christi K. Madsen. Design of a hybrid As_2s_3-Ti:LiNbO_3 optical waveguide for phase-matched difference frequency generation at mid-infrared. *Optics Express*, 22(22):27183, November 2014.

[36] Roel Baets, Roel Baets, Ananth Z. Subramanian, Ananth Z. Subramanian, Stéphane Clemmen, Stéphane Clemmen, Bart Kuyken, Bart Kuyken, Peter Bienstman, Peter Bienstman, Nicolas Le Thomas, Nicolas Le Thomas, Günther Roelkens, Günther Roelkens, Dries Van Thourhout, Dries Van Thourhout, Philippe Helin, and Simone Severi. Silicon Photonics: silicon

nitride versus silicon-on-insulator. In *Optical Fiber Communication Conference (2016), paper Th3J.1*, page Th3J.1. Optical Society of America, March 2016.

[37] Implementation of optical switches using mzi. 2018.

[38] M. Romagnoli. Highly Efficient Silicon Photonics Phase Modulator using Graphene. In *2018 Optical Fiber Communications Conference and Exposition (OFC)*, pages 1–3, March 2018.

[39] V. Sorianello, G. De Angelis, T. Cassese, M. Midrio, M. Romagnoli, M. Mohsin, M. Otto, D. Neumaier, I. Asselberghs, J. Van Campenhout, and C. Huyghebaert. Complex effective index in graphene-silicon waveguides. *Opt. Express*, 24(26):29984–29993, December 2016.

[40] Zhe Qi, Zhi Hong Zhu, Wei Xu, Jian Fa Zhang, Chu Cai Guo, Ken Liu, Xiao Dong Yuan, and Shi Qiao Qin. Electro-optic switching based on a waveguide-ring resonator made of dielectric-loaded graphene plasmon waveguides. *Applied Physics Express*, 9(9):092001, 2016.

[41] Surface roughness, mitutoyo.com.

[42] Yixiao Gao and Ilya V. Shadrivov. Nonlinear coupling in graphene-coated nanowires. *Scientific Reports*, 6:38924, December 2016.

# Appendices

# Appendix A

# Waveguide mode calculation

Given the following parameters:

| | |
|---|---|
| $n_{core} = 3.48$ | refractive index of the core |
| $n_s = 1.44$ | refractive index of the substrate |
| $n_c = 1.44$ | refractive index of the cover |
| $h = 0.22\mu m$ | height of the core |
| $\lambda = 1.55\mu m$ | central wavelength |
| $k = 2\pi/\lambda$ | wave vector |
| $\kappa_{max} = \sqrt{(k \cdot n_{core})^2 - (k \cdot n_s)^2}$ | (See Figure A.1) |
| $\beta = \sqrt{(k \cdot n_{core})^2 - \kappa^2}$ | (See Figure A.1) |
| $\gamma_s = \sqrt{\beta^2 - (k \cdot n_s)^2}$ | |
| $\gamma_c = \sqrt{\beta^2 - (k \cdot n_c)^2}$ | |

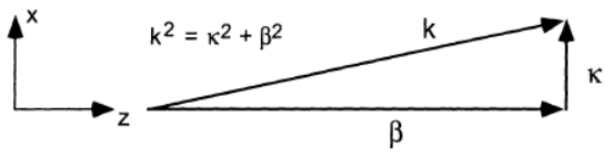


Geometric relation between $\beta$, $\kappa$, and $k$.

Figure A.1

The number of existing modes in the waveguide can be found as the number of solutions in the following 2 transcendental equations:

$$TM: \qquad tan(h\cdot\kappa) = \frac{\kappa\cdot\left(\frac{n_{core}^2}{n_c^2}\gamma_c + \frac{n_{core}^2}{n_s^2}\gamma_s\right)}{\kappa^2 - \frac{n_{core}^4}{n_c^2 n_s^2}\cdot\gamma_c\cdot\gamma_s} \tag{A.1}$$

$$TE: \qquad tan(h\cdot\kappa) = \frac{(\gamma_c+\gamma_s)}{\kappa\cdot(1-\frac{\gamma_c\cdot\gamma_s}{\kappa^2})} \tag{A.2}$$

These transcendental equations (A.2,A.1) have each only one solution in $\kappa \in [0, \kappa_{max}]$ as long as $h < 220\,nm$.
The same method applied in the other transversal direction yields $b < 500\,nm$. When we go below these values, not only do we lose a lot of guided light to radiating modes, but also surface roughness for dimensions close to lower cutoff brings along a lot of losses [41]. Very commonly used in this field are the dimensions 220 x 450 nm, which I will also use.

# Appendix B

# Graphene-light interaction

Using Poynting's theorem of energy conservation in lossy media, the absorbed portion of optical power $Q_s$ in a sheet of graphene is completely converted to heat due to resistive dissipation (Ohmic losses). In equations expressed, this reads as:

$$\int_S \langle Q_S \rangle \cdot dr^2 = \frac{1}{2} \int_S J_S \cdot E_t \cdot dr^2 = \frac{\sigma_0}{2} \int_S |E_t^2| \cdot dr^2 \tag{B.1}$$

where $\sigma_0 = \frac{e^2}{4\hbar}$ is the AC conductance of graphene for interband transition, $E_t$ is the in-plane component of the transverse electric field, $J_s$ is the induced surface current. $Q_s$ is the time-averaged resistive dissipation per unit area and the surface integral is performed over the surface of graphene S. Application of this relation to normal incidence with input optical intensity of:

$$I_{inc} = \varepsilon_0 \cdot c \frac{|E_t^2|}{2}$$

gives the non-wavelength dependent absorption coefficient of:

$$\frac{Q_s}{I_{inc}} = 2.3\%$$

Because this value is very little affected by many parameters,such as the Fermi-level of graphene, we cannot manipulate it easily, which is yet another reason why we don't use this perpendicular configuration for electro-modulated switching.
In the coplanar graphene-on-waveguide configuration however, the dissipation $\langle Q_s \rangle$ leads to a linear absorption coefficient as given by:

$$\alpha = -\frac{1}{P(z)} \cdot \frac{dP(z)}{dz} = \frac{1}{P(z)} \cdot \int_L \langle Q_s(x) \rangle dl = \frac{\sigma_0}{2P(z)} \cdot \int_L |E_t(x, y_0)|^2 dz \tag{B.2}$$

Here, z is the propagation direction. The graphene layer has width L and is at height $y_0$.

For the quasi-TE mode of the waveguide, the transverse electrical field $E_t$ in the graphene consists predominantly of the $E_z$ component which decays exponentially as a function of distance y outside the waveguide. Because the graphene resides in the evanescent field of the waveguide mode, the absorption coefficient decreases exponentially with $y_0$ as:

$$\alpha(y_0) = \alpha_0 \cdot e^{-2\gamma y_0} \tag{B.3}$$

where $\gamma$ is the field decay constant outside the waveguide, which of course depends on the height of the waveguide and the oxide layer.